Specification and survival of post-metamorphic branchiomeric neurons in the hindbrain of a non-vertebrate chordate.

Eduardo D. Gigante, Katarzyna M. Piekarz, Alexandra Gurgis, Leslie Cohen, Florian Razy-Krajka, Sydney Popsuj, Hussan S. Ali, Shruthi Mohana Sundaram, Alberto Stolfi

School of Biological Sciences, Georgia Institute of Technology, Atlanta, GA, USA 30332

Author for correspondence: alberto.stolfi@biosci.gatech.edu

Abstract:

Tunicates are the sister group to the vertebrates, yet most species have a life cycle split between swimming larva and sedentary adult phases. During metamorphosis, larval neurons are largely replaced by adult-specific ones. Yet the regulatory mechanisms underlying this neural replacement remain largely unknown. Using tissue-specific CRISPR/Cas9-mediated mutagenesis in the tunicate *Ciona*, we show that orthologs of conserved hindbrain and branchiomeric neuron regulatory factors Pax2/5/8 and Phox2 are required to specify the "Neck", a compartment of cells set aside in the larva to give rise to cranial motor neuron-like neurons in the adult. Using bulk and single-cell RNAseq analyses, we also characterize the transcriptome of the Neck downstream of Pax2/5/8. Surprisingly, we find that Neck-derived adult ciliomotor neurons begin to differentiate in the larva, contrary to the long-held assumption that the adult nervous system is formed only after settlement and the death of larval neurons during metamorphosis. Finally, we show that manipulating FGF signaling during the larval phase alters the patterning of the Neck and its derivatives. Suppression of FGF converts Neck cells into larval neurons that fail to survive metamorphosis, while prolonged FGF signaling promotes an adult neural stem cell-like fate instead.

Introduction

The simple embryos of the non-vertebrate chordate *Ciona* and related tunicates comprise a highly tractable system in which to study the regulation of cellular processes in development (Bernadskaya and Christiaen, 2016; Cao et al., 2019; Farley et al., 2015; Guignard et al., 2020; Wang et al., 2019). Their classification as tunicates, the sister group to the vertebrates (Delsuc et al., 2006), means they share with vertebrates many chordate-specific gene families, cell types, organs, and anatomical structures (Abitua et al., 2015; Christiaen et al., 2002; Di Gregorio, 2020; Dufour et al., 2006; Fodor et al., 2021; Lemaire et al., 2021; Papadogiannis et al., 2022; Razy-Krajka et al., 2014; Stolfi et al., 2015). The simplicity of their embryos overshadows the fact that the larva is but one part of a biphasic life cycle alternating between a free-swimming larval phase and a sessile adult phase (**Figure 1A**). During metamorphosis, larval structures degenerate and are replaced by adult tissues and organs (Nakayama-Ishimura et al., 2009; Sasakura and Hozumi, 2018). Although the invariant cell lineages and gene regulatory networks specifying many of the embryonic cell types of *Ciona* have been investigated in detail (Cao et al., 2019; Imai et al., 2006), metamorphosis and adult development are still poorly understood. We know that various undifferentiated progenitor cells set aside in the larva as discrete compartments can give rise to adult structures (Dufour et al., 2006; Horie et al., 2011; Razy-Krajka et al., 2014; Sasakura and Hozumi, 2018). These adult progenitor cells are patterned and specified in an invariant manner alongside differentiated larval cells, but only fully differentiate after the larva finds a location to settle and undergo metamorphosis. This transition from invariant (stereotyped) to variable (plastic) development is unique among the chordates, and thus of potential interest for revealing previously unknown mechanisms for precise spatiotemporal regulation of cellular quiescence, survival, proliferation, and differentiation.

In this work, we focused on a specific compartment of *Ciona* adult neural precursor cells in the larva called the “Neck” (**Figure 1B,C**). Based on their expression of conserved regulatory genes such as *Pax2/5/8.a, Phox2,* and *Hox1* (**Figure 1C,D**), it has been proposed that the Neck is homologous to part of the vertebrate hindbrain, specifically those cells giving rise to branchiomeric efferents, such as branchiomeric motor neurons (Dufour et al., 2006; Hudson and Yasuo, 2021). Although the Neck is specified during embryonic development and shares a close developmental lineage with differentiated larval brain neurons (**Figure 1B-D**), most of it remains in an undifferentiated state until after metamorphosis (Dufour et al., 2006; Imai et al., 2009). Despite their shared origins, larval neurons degenerate during metamorphosis, while neural progenitors in the Neck and in other compartments appear to survive into the adult phase (**Figure**

63 **1D**) (Horie et al., 2011; Hozumi et al., 2015). However, the signaling pathways and regulatory
64 networks that direct Neck specification, survival, and differentiation remain uncharacterized.

65 Here we investigate the molecular mechanisms underlying the specification and patterning
66 of the Neck from embryogenesis to post-metamorphic development. We show that the Neck cells
67 continue to divide throughout embryogenesis and the larval phase, with some of their derivatives
68 differentiating into larval- and adult-specific neurons. We show that Pax2/5/8.a and Phox2 are
69 required for the specification of Neck-derived adult neurons, and that FGF signaling regulates the
70 balance of differentiation and proliferation/survival in the Neck during the transition between larval
71 and adult phases. Thus, we reveal key molecular mechanisms underlying the ability of *Ciona* to
72 generate an entirely separate adult nervous system even as its larval nervous system is largely
73 eliminated.

74

75 **Methods**

76 **Ciona handling, fixation, staining, and imaging.**

77 Adult *Ciona robusta* (*intestinalis* Type A) were collected from San Diego, CA (M-REP).
78 Dechorionated zygotes were generated and electroporated as previously described (Christiaen
79 et al., 2009a, b). Embryos were raised in artificial sea water at 20°C. Animals raised beyond 24
80 hours post-fertilization (hpf) were moved to new agarose coated plates with fresh artificial sea
81 water +1.0% Penicillin-Streptomycin (Gibco) daily. Post-metamorphic animals were paralyzed
82 with L-menthol prior to fixation, as previously described (Osugi et al., 2020). Staging is based on
83 TUNICANATO database (Hotta et al., 2020). Cell lineage nomenclature is based on Conkin
84 (Conklin, 1905; Nicol and Meinertzhagen, 1991). All sequences of plasmids, probes, and sgRNAs
85 not previously published can be found in the Supplemental Sequences file.

86 Sample processing for fluorescence and immunostaining were performed as previously
87 described (Beh et al., 2007; Ikuta and Saiga, 2007; Stolfi et al., 2011). Unc-76-tagged GFP and
88 mCherry (Dynes and Ngai, 1998) were used to improve labelling of cell bodies and axons, instead
89 of GFP/mCherry alone. An Unc-76-tagged StayGold green fluorescent protein was also designed
90 and used for its improved signal longevity (Hirano et al., 2022). Immunolabeling of Cas9 protein
91 by monoclonal anti-mouse Cas9 antibody at 1:500 (4G10; Diagenode) was blocked in PBS Super
92 Block (37580; ThermoFisher) and visualized with goat anti-mouse AlexaFluor 568 (Invitrogen).
93 Juvenile animals stained with phalloidin-AlexaFluor 405 or 647 (ThermoFisher; A30104, A22287).

In situ hybridization coupled to immunostaining was performed as previously described (Beh et al., 2007), using TSA Plus amplification kits (Akoya Biosciences) and mouse anti-β-galactosidase (Promega #Z378, 1:1000) or rabbit anti-mCherry (BioVision, accession number ACY24904, 1:500) primary antibodies. Two-color (Fluorescein + Cy3) double *in situ* hybridization was performed using TSA Plus amplification kits as previously described (Ikuta and Saiga, 2007; Stolfi et al., 2011). Probe template sequences can be found in the Supplemental Sequences file. All standard images were captured on a Leica epifluorescence compound microscope. Confocal images were captured on a Nikon AX R with NSPARC and processed in ImageJ (1.54d). Phenotypes were quantified on a Leica DMi8 or DMIL LED inverted epifluorescence microscope. Biological replicates are presented in side-by-side graphs generated in Prism (9.5.1). Cell count data analyzed by one-way ANOVA and Dunnett's test of multiple comparisons.

CRISPR/Cas9 sgRNA design and validation

Single-chain guide RNAs (sgRNAs) were designed using CRISPOR (http://crispor.tefor.net/) and vectors were constructed as previously described (Gandhi et al., 2018; Haeussler et al., 2016) or custom synthesized and cloned (Twist Bioscience). Individual sgRNA vectors were validated *in vivo* as previously described (Johnson et al., 2023) with a ubiquitous *Eef1a -1955/-1>Cas9* or *Eef1a -1955/-1>Cas9::Geminin (Johnson et al., 2023; Stolfi et al., 2014)*. Genomic DNA was isolated using QiaAMP Micro extraction kit (QIAGEN), targeted regions amplified by PCR using AccuPrime Pfx (ThermoFisher), and PCR products purified using the QiaQuick PCR Purification kit (QIAGEN) following the published protocol (Johnson et al., 2023). Samples were sequenced using commercial Illumina-based amplicon sequencing (Amplicon-EZ; Azenta) and efficiency was determined by indel % compared to controls. Data on sgRNA efficiency is provided in **Supplemental Figure 5** and sgRNA sequences are provided in the **Supplemental Sequences** file.

Bulk RNA sequencing

Fertilized zygotes were prepared and electroporated as described above. Zygotes were electroporated with DNA plasmids using a pan-neuronal driver *Nut -1155/-1 (Johnson et al., 2023; Shimai et al., 2010)*: *Nut-1>LacZ Control*, *Nut-1>Pax2/5/8.a transcript variant 1 ("tv1",* transcript model *KY21.Chr6.690.v2.SL1-1)*, or *Nut-1>Pax2/5/8.a transcript variant 2 ("tv2",* transcript model

125 *KY21.Chr6.690.v2.SL1-1*). Experiment was repeated in duplicate. RNA was isolated from 10 hpf
126 embryos using a Monarch total RNA miniprep kit (New England BioLabs Inc.) RNA was stored at
127 -80°C until sample analysis and sequencing by the Molecular Evolution Core at Georgia Tech as
128 previously reported (Johnson et al., 2023). Briefly, total RNA integrity levels were measured by
129 the Agilent Bioanalyzer RNA 6000 Nano kit and all samples had RINs above 9. Enrichment for
130 mRNAs was performed using the NEBNext Poly(A) mRNA isolation modulate and Illumina
131 libraries were prepared by the NEBNext Ultra II RNA directional library preparation kit. Libraries
132 were pooled and sequenced on the NovaSeq 6000 with an SP Flow Cell, to obtain PE100bp
133 reads. Pax2/5/8.a transcriptional variant fold change Pearson Correlation analysis and graph
134 generated in Prism (9.5.1).

135 Data quality control and analysis were performed in Galaxy (usegalaxy.org) (Community, 2022).
136 Raw reads were quality controlled with FastQC and Cutadapt. Reads were mapped to the
137 HT_KY21 *Ciona robusta* genome with RNA STAR and checked using the Integrative Genomics
138 Viewer (IGV; Version 2.14.1)(Satou et al., 2005; Satou et al., 2022). The number of reads per
139 annotated genes were counted using featureCounts and DESeq2 was then used on the read
140 counts to normalize them to the controls. Datasets were then annotated with the HT_KY21
141 genome (Satou et al., 2022). KY21 gene models were linked to KH gene models using the Ciona
142 Gene Model Converter https://github.com/katarzynampiekarz/ciona_gene_model_converter. For
143 each step, quality reports were aggregated using MultiQC. Raw FASTQ files can be found in the
144 SRA database under BioProject accession number PRJNA981160. Analyzed data is provided in
145 **Supplemental Table 1**.

146

147 **Single-cell RNA sequencing reanalysis**

148 Re-processed scRNAseq data from Cao et al. 2019 were analyzed (Cao et al., 2019;
149 Johnson et al., 2023). Data from *Ciona* embryos in the Mid-tailbud II stage, roughly 10 hours post-
150 fertilization (hpf) were analyzed using the Seurat v3 package in R to identify cell type clusters
151 based on unique gene expression markers (**Supplemental Figure 4A**) (Satija et al., 2015; Stuart
152 et al., 2019). Replicates were integrated and pre-processing and clustering were performed using
153 the SCtransform and FindMarker functions (Hafemeister and Satija, 2019). Cluster 25 was
154 identified as containing Neck cells based on high enrichment for *Pax2/5/8.a* reads (**Supplemental**
155 **Figure 4B, Supplemental Table 2**). Cluster 25 cells were re-clustered based on differential gene
156 expression, resulting in two sub-clusters (see **results**). The FeaturePlot function was used to

157 visualize feature expression in low-dimensional space, and to use colors to map out the relative
158 expression levels for each gene of interest in the Neck and brain clusters. Additionally, VlnPlot
159 and RidgePlot functions were applied to the expression distributions within the clusters, allowing
160 for the heterogeneity of the Neck cluster to be further examined and the potential for additional
161 sub-populations noted. R objects and code can be accessed on OSF at https://osf.io/uc32x/.

162

163 **RT-PCR of Phox2 cDNA**

164 RNA was isolated from 17 hpf *Ciona robusta* larvae by Monarch Total RNA miniprep kit
165 (New England BioLabs Inc.). cDNA was produced by Omniscript reverse transcription kit
166 (QIAGEN). The resulting cDNA was diluted in nuclease-free water and stored at -20C. Based on
167 the RNA model discovered during RNA sequence analysis, forward (5'-
168 CATAACGATGGACTACCCTGC) and reverse primers (5'-CAGACATGTCGTGGTAGGATAGG)
169 targeting the new exon 1 of *Phox2* and stop site of *KY21.CH14.159*, respectively, were used to
170 perform PCR on the single strand cDNA with OneTaq 2X Master Mix (NEB, M0482S) in 50 µL
171 reactions with a touchdown PCR program. PCR products were purified (QIAquick PCR
172 purification kit; QIAGEN) and TOPO-cloned into dual promoter empty vector (ThermoFisher,
173 450640). White colonies grown on LB plates with 100 mg/mL ampicillin and coated with X-Gal
174 were selected and tested for an insert of correct size by restriction enzyme digest. Plasmids of
175 the appropriate size were sequenced by Sanger sequencing with M13 forward and reverse
176 primers.

177

178 **Results**

179 **A time-series description of the "Neck" lineage through development and metamorphosis**

180 Presently, the *C. robusta* Neck has been described as 6 ependymal cells per side, thought
181 to be quiescent in nature, and a bilateral pair of differentiated neurons, the so-called "Neck
182 Neurons" (Ryan et al., 2016, 2017). To establish how the Neck lineage develops between early
183 tailbud and hatched larval stage, we examined Neck cell number, cell type, and morphology using
184 *Pax2/5/8.a* (Oonuma et al., 2021) and *Phox2* (Dufour et al., 2006) fluorescent reporters at hourly
185 intervals, in embryos raised at 20°C (**Figure 2A-J**).

186 At the early tailbud stage (Hotta Stage 19, ~9 hpf), two *Pax2/5/8.a>H2B::mCherry+*
187 positive cells on either left/right side of the embryo can be observed, corresponding to A11.61

188 and A11.62 (**Figure 2A**). These two cells continue to divide, forming a single line of four cells on
189 either side by the mid-tailbud stage (St. 20-22, ~9-10 hpf, **Figure 2B**). By this stage, the middle
190 cells (A12.122 and A12.123) start to express *Phox2>GFP*, whereas the most anterior and
191 posterior cells (A12.121 and A12.124) do not (**Figure 2C**). Starting at Stage 23 (~11 hpf), the
192 posteriormost cell (A12.121) divides first, (**Figure 2D**), followed by the anteriormost cell (A12.124)
193 dividing around Stage 24 (~12 hpf, **Figure 2E**). This brings the total number of *Pax2/5/8.a*+ cells
194 on either side to six. These six Neck cells have not yet differentiated at this stage and maintain a
195 typical ependymal cell morphology within the neural tube epithelium. Although the cells appear to
196 divide in a stereotyped order, the exact timing of their divisions is slightly variable from embryo to
197 embryo and even between left/right sides in the same individual (**Supplemental Figure 1A**).

198 During the late tailbud stage (St. 25, ~14 hpf), the Phox2+ cells (A12.122 and A12.123)
199 divide, resulting in four cells labeled by *Phox2>GFP* (**Figure 2F**). The posterior, *Phox2*-negative
200 cells also divide around this time and appear to delaminate from the neural tube epithelium,
201 separating from the *Phox2*+ cells (**Figure 2F,G**). Beyond stage 26 (larval stages, ~16 hpf
202 onwards), additional cell divisions are seen among the *Phox2*>GFP+ cells, as well as the anterior
203 *Phox2*-negative cells. This increases the number of *Pax2/5/8.a*+ cell to an average of 12 on each
204 side but the order of divisions and lineage are not easily traced (**Figure 2G**,**H**). Furthermore,
205 *Phox2>GFP* expression expands anteriorly in the lineage during the larval phase but is not
206 detectable in the posterior cells that have delaminated from the neural tube epithelium (**Figure**
207 **2G**). The average number of *Pax2/5/8.a*+ Neck cells was quantified at each developmental stage
208 and is reported in **Figure 2H**. Based on these data, Neck cells continue to divide into the larval
209 stage, suggesting they are not as quiescent as previously assumed (Imai et al., 2009).

210 During the larval stages we observed the differentiation of the posteriormost cell of the
211 lineage on either side, likely the "Neck Neuron" as previously described (Ryan et al., 2016,
212 2017)(**Figure 2I**). However, we also observed *Pax2/5/8.a>GFP*+ neurites extending from cells
213 just anterior to the Neck Neuron (**Figure 2J**). In early post-metamorphic juveniles (St. 37, 38, ~72-
214 95 hpf) we observed neurons labeled by *Phox2* and *Pax2/5/8.a* reporters innervating the gill slits
215 (**Figure 2K,L; Supplemental Figure 1B; Supplemental Video 1**), similar to those reported
216 previously (Dufour et al., 2006), and presumably correspond to the cholinergic ciliomotor neurons
217 (CMNs) that control branchial ciliary flow (Jokura et al., 2020). Based on their position, axon
218 trajectory, and expression of *Pax2/5/8.a,* these CMNs are likely to correspond to the early
219 differentiating neurons whose nascent axons can be seen extending towards the future gill slits
220 (**Figure 2J**).Together, these observations suggest that the adult nervous system begins to

221 differentiate before metamorphosis and the degeneration of the larval nervous system. This was
222 surprising given the traditional assumption that larval neurons are eliminated during
223 metamorphosis, while adult neurons arise from set-aside, undifferentiated progenitors. Our
224 results suggest a less clear contrast between pre- and post-metamorphic neurogenesis in
225 tunicates. An updated model of the Neck cell lineage and its derivatives is proposed in **Figure**
226 **2M**.

227

228 **Pax2/5/8 and Phox2 orthologs are required for the formation of Neck-derived neurons.**

229 Having established that the Neck lineage likely gives rise to gill slit-innervating CMNs, we
230 next tested the roles of *Pax2/5/8.a* and *Phox2* in establishing these post-metamorphic neurons.
231 More specifically, we used CRISPR/Cas9 gene editing and gene-specific sgRNAs to disrupt either
232 gene in neural progenitors prior to hatching and metamorphosis. Embryos were electroporated
233 with "negative control" or gene-specific sgRNA expression plasmids, *Sox1/2/3>Cas9::Geminin*$^{N-}$
234 ^{ter} plasmid to drive expression of Cas9 in neural progenitors, and a *Phox2>GFP* reporter to label
235 post-metamorphic CMNs. Animals were grown to Stage 37 (~72 hpf) and imaged to assay the
236 presence of CMNs. In negative control animals, *Phox2>GFP*+ CMNs were observed in a majority
237 of animals (**Figure 3A,D**). In contrast, disrupting either *Pax2/5/8.a* or *Phox2* by CRISPR resulted
238 in drastic loss of *Phox2>GFP*+ CMNs, as evidenced by lack of axons innervating the gill slits
239 (**Figure 3B-D**). This suggests that Pax2/5/8.a and Phox2 are necessary for the specification and
240 differentiation of post-metamorphic CMNs, supporting their origins from the Neck lineage in which
241 both transcription factors are initially detected.

242 To understand how overexpression of Pax2/5/8.a impacts the developing nervous system,
243 we expressed *Pax2/5/8.a* transcriptional variant 1 (*tv1*) under control of the pan-neuronal Nut
244 driver (*Nut>Pax2/5/8.a*) and examined *Phox2>GFP*+ cells in the Stage 36 juvenile (~72 hpf). In
245 *Nut>LacZ* negative controls, *Phox2>GFP*+ CMNs innervate the early gill slits as expected (**Figure**
246 **3E**). In animals overexpressing Pax2/5/8.a, we observed an expansion of Phox2+ cells
247 throughout the juvenile brain region, but no change in the presence or number of gill slit-
248 innervating CMN axons (**Figure 3F**). Together, this suggests that Pax2/5/8.a is sufficient to
249 activate Phox2 expression in the post-metamorphic CNS, but might not be sufficient to impart a
250 CMN identity.

251

252 **Characterizing the transcriptional program downstream of Pax2/5/8 by RNAseq**

253 Because Pax2/5/8.a appeared to be a key regulator of Neck identity, we sought to identify
254 its potential downstream transcriptional targets. To do this, we measured global transcriptome
255 changes by bulk RNA sequencing (RNAseq). We used the *Nut* promoter (Shimai et al., 2010) to
256 overexpress both isoforms of *Pax2/5/8.a* (transcript variants "tv1" and "tv2") throughout the neural
257 tube, and compared whole-embryo transcriptomes of Pax2/5/8.a-overexpression and negative
258 control (no overexpression) embryos at 10 hpf. Differential gene expression analysis revealed the
259 enrichment, or depletion, of transcripts upon overexpression of either Pax2/5/8.a variant (**Figure**
260 **4A, Supplemental Table 1**). Previously known Neck markers and Pax2/5/8.a targets (e.g. *Phox2,*
261 *Gli, Eph.c, FGF9/16/*20) were among the top 600 upregulated genes (out of ~16,000), with some
262 being considerably higher in ranking (e.g. *Phox2*). In contrast, several known markers of the brain
263 and Motor Ganglion were among the top 50 genes most *downregulated* by Pax2/5/8.a (e.g. *Pax6,*
264 *Nk6, Neurogenin, BCO).* Correlation between differential gene expression values elicited by the
265 two isoforms was modestly high (Pearson Correlation r = 0.70) (**Supplemental Figure 2**),
266 suggesting high reproducibility and specificity of the Pax2/5/8.a-downstream effects.

267 One gene previously known to be downstream of Pax2/5/8.a in the Neck, *Gli* (Imai et al.,
268 2009), was among the top 31 upregulated genes using either Pax2/5/8.a isoform (**Figure 4A**).
269 Indeed, CRISPR/Cas9-mediated knockout of *Pax2/5/8.a* largely abolished *Gli>GFP* reporter
270 expression in the Neck, confirming that it is downstream of Pax2/5/8 (**Figure 4B-D**). Following the
271 same approach, we were able to validate a novel putative target of Pax2/5/8.a, the gene *Vanabin4*
272 (*Van4,* gene IDs *KH.C3.88/KY21.Chr3.256*). *Van4* encodes a tunicate-specific vanadium-binding
273 protein and was among the top 1-2 upregulated genes by both isoforms of Pax2/5/8.a (**Figure**
274 **4A**). *In situ* mRNA hybridization revealed expression of *Van4* specifically in the Neck (**Figure 4E**).
275 *Van4* expression was lost upon *Pax2/5/8.a* CRISPR knockout (**Figure 4F**), and expanded
276 throughout the neural tube upon overexpression of Pax2/5/8.a (**Figure 4G**). *Van4>GFP* reporter
277 expression in the Neck was similarly lost upon *Pax2/5/8.a* CRISPR knockout (**Figure 4H-J**).
278 Taken together, these data reveal a transcriptional program for Neck specification downstream of
279 Pax2/5/8.a in *Ciona.*

280

281 **Correcting the *C. robusta Phox2* gene model.**

282 During analysis of RNA sequencing data, we observed upregulation of *Phox2*
283 (*KY21.Chr14.160*) and neighboring gene *KY21.Chr14.159* by Pax2/5/8.a overexpression. On

closer inspection of our bulk RNA sequencing, we found that reads spanned exons covering both gene models, and further revealed two cryptic exons (exon 1 and exon 5)(**Figure 5A,B**). A corrected, consolidated gene model (**Figure 5C**) was supported by sequencing a full-length Phox2 cDNA clone spanning all 7 exons, cloned from 17 hpf larvae (**Supplemental Figure 3A**), and by protein sequence alignment with predicted Phox2 protein models from other tunicate species (**Supplemental Figure 3B**). Finally, mRNA *in situ* hybridization using probes designed for both *Chr14.160* and *Chr14.159* gene models revealed identical expression patterns specific to the Neck, further supporting the finding that these are indeed the same gene (**Figure 5D**). The function of the extended C-terminus (which is divergent relative to that of vertebrate Phox2 family members) is unknown, but will likely be important for future studies on transcriptional regulation by Phox2.

Characterization of Neck cell transcriptomes in single-cell RNAseq data.

To further characterize the molecular profiles of Neck cells, we re-analyzed published whole-embryo single-cell RNA sequencing (scRNAseq) data obtained at the mid-tailbud II stage (Cao et al., 2019). This revealed a single cluster enriched for *Pax2/5/8.a* reads (cluster 25, **Figure 6A, Supplemental Figure 4A,B, Supplemental Table 2**). Re-clustering performed only on cluster 25 cells revealed two distinct subclusters, with *Pax2/5/8.a* enriched in one subcluster (subcluster 0) and depleted in the other (subcluster 1)(**Figure 6B, Supplemental Figure 4C**). Double *in situ* hybridization using probes for *Pax2/5/8.a* and a top subcluster 1 marker *Crls1 (KH.C11.724)* confirmed that subcluster 0 represents the Neck, while subcluster 1 appears to represent larval brain neurons and photoreceptors just anterior to the Neck (**Figure 6C**). Other markers enriched in subcluster 0 cells further confirmed their identity as Neck cells, showing substantial overlap with the top genes upregulated by Pax2/5/8.a overexpression as measured by our bulk RNAseq experiment above (**Figure 6D,E Supplemental Table 3**). Correlation between enrichment/depletion in the Neck by scRNAseq and average upregulation/downregulation by Pax2/5/8.a was modest (Pearson correlation = 0.43; Spearman's rank correlation = 0.46)(**Supplemental Table 4**). We observed notable exceptions, such as *Hox1,* which is highly expressed in the Neck but was not upregulated by Pax2/5/8.a (**Figure 6D,E**). This suggests that Pax2/5/8.a is not sufficient to activate the entirety of the transcriptional program of the Neck, and that some important Neck regulators might be expressed in parallel to, not downstream of, Pax2/5/8.a. In contrast, the top markers enriched in the “brain” subcluster (subcluster 1) were among those transcripts most highly depleted by Pax2/5/8.a overexpression,

317 suggesting that Pax2/5/8.a is also instrumental for repressing larval brain neuron/photoreceptor
318 identity.

319 As expected, *Phox2* expression (represented by the KH.C14.119/KY21.Chr14.159 gene
320 model, due to the 3' bias of 10X Genomics system) was unevenly distributed within subcluster 0.
321 *Phox2* was expressed more highly in one half of the subcluster than in the other half (**Figure 6F**),
322 recapitulating its expression in a subset of Neck cells as seen by *Phox2>GFP* expression.
323 Additional genes showed a similar distribution in Neck subcluster (e.g. *Rspo3, Tesk,* **Figure 6F,**
324 **Supplemental Figure 4D**), further confirming the distinction between
325 proliferating/undifferentiated cells in the anterior Neck and differentiating Neck-derived neurons
326 in the posterior.

327

328 **Ephrin/Eph and FGF signaling regulate the balance between proliferation and**
329 **differentiation.**

330 FGF/MAPK signaling plays numerous, recurring roles in the development of the *Ciona*
331 larval nervous system (Davidson et al., 2006; Haupaix et al., 2013; Razy-Krajka et al., 2018; Stolfi
332 et al., 2011). In fact, FGF8/17/18 from the neighboring A9.30 cell lineage is required for expression
333 of *Pax2/5/8.a,* which in turn activates expression of *FGF9/16/20* in the Neck (**Figure 7A**) (Imai et
334 al., 2009). Furthermore, Ephrin/Eph signaling antagonizes FGF/MAPK signaling to provide crucial
335 spatial information for FGF/MAPK-dependent patterning and cell fate choice in the nervous
336 system, including in the Motor Ganglion (MG), in which downregulation of FGF/MEK promotes
337 cell cycle exit and neuronal differentiation (Haupaix et al., 2013; Stolfi et al., 2011). Expression of
338 *FGF9/16/20* and *Eph.c* (formerly *Eph3*) in the Neck (**Figure 7A,B**), and *EphrinA.b* and *EphrinA.d*
339 (**Figure 7C,D**) in the cells of the brain and MG abutting the Neck suggested that FGF and
340 Ephrin/Eph signaling might be key to regulating cell fate and neuronal differentiation in the Neck
341 as well.

342 To test the role of FGF and Ephrin signaling in the Neck, we used the *Pax2/5/8.a* promoter
343 to overexpress dominant-negative FGF receptor (dnFGFR), dominant negative Eph.c receptor
344 (dnEph.c), or a constitutively-active form of the MAPK kinase MEK ($MEK^{S220E,S216D}$, also called
345 caMEK) (Davidson et al., 2006; Picco et al., 2007; Razy-Krajka et al., 2018; Shi and Levine, 2008).
346 We examined the Neck at the late swimming larval stage (St. 29), when there are ~8 anterior
347 putatively undifferentiated, neuroepithelial cells and ~4 posterior, differentiating neurons in control
348 larvae (**Figure 7E,I,J**). In larvae expressing the dnFGFR, we observed fewer cells overall in the

349 Neck, and undifferentiated cells appeared to be replaced by supernumerary neurons, as
350 evidenced by loss of epithelial organization and excess axon outgrowth (**Figure 7F,I,J**). This
351 contrasted starkly with larvae expressing the dnEph.c, in which we observed a near-complete
352 loss of differentiated neurons, most clearly evidenced by a distinct absence of the posterior Neck
353 Neuron axon extending towards the tail (**Figure 7G,I,J**). Instead, the entire Neck took on the
354 morphology of undifferentiated neural precursors in a tightly-packed neuroepithelium. This was
355 phenocopied by caMEK, which constitutively activates the FGF/MAPK pathway in all cells (**Figure**
356 **7H,I,J**). We observed these phenotypes, consistently across two biological replicates (**Figure**
357 **7I,J**). Taken together, these results suggest that Ephrin/Eph-mediated suppression of FGF/MAPK
358 signaling is sufficient and necessary for neuronal differentiation in the Neck, and that sustained
359 FGF/MAPK signaling promotes an undifferentiated, neuroepithelial state instead.

360 We also examined the expression of *Phox2>GFP* in the Neck, which is normally
361 expressed by the ependymal-like cells in the middle part of the Neck (**Figure 7K**). As expected,
362 we observed a loss of Phox2+ Neck cells in larvae electroporated with *Pax2/5/8.a>dnFGFR*
363 (**Figure 7L,O**). However, neither *Pax2/5/8.a>dnEph.c* nor *Pax2/5/8.a>caMEK* abolished
364 *Phox2>GFP* expression but rather made its spatial distribution within the Neck inconsistent
365 (**Figure 7M-O**). This suggests that sustained FGF/MEK signaling is permissive but not sufficient
366 for *Phox2* activation in the Neck.

367 Because our data had revealed upregulation of genes encoding the BMP antagonist
368 Noggin and the Hedgehog (Hh) pathway effector Gli, downstream of Pax2/5/8.a (**Figure 4,**
369 **Supplemental Table 4**), we also tested the effects of perturbing these pathways. No significant
370 effect on Neck morphogenesis was observed upon overexpression of dominant-negative or
371 constitutive BMP receptors (**Figure 8A-D**) or CRISPR/Cas9-mediated knockout of *Gli* (**Figure 8E-**
372 **G**). While these results do not rule out a role for BMP and/ Hh signaling pathways in the
373 development of the Neck or Neck-derived neurons, they do not impact the balance of
374 differentiation and proliferation like Ephrin and FGF do.

375 Finally, because disruption of Ephrin/FGF/MAPK signaling significantly impacted cell
376 proliferation and differentiation in larvae, we examined how these perturbations affected the
377 development of CMNs in post-metamorphic juveniles. We observed a loss of Pax2/5/8.a>GFP+
378 CMN axons in juveniles that had expressed the dnFGFR receptor in the Neck at the larval stage
379 (**Figure 9A,B**), but not in animals that expressed dnEph.c or caMEK (**Figure 9C,D**). We conclude
380 that the supernumerary, differentiating neurons seen in the larvae generated by
381 *Pax2/5/8.a>dnFGFR* do not survive metamorphosis, failing to give rise to fully differentiated

382 CMNs in the juvenile. In contrast, undifferentiated neuroepithelial cells elicited by dnEph.c or
383 caMEK overexpression still retain the potential to differentiate into CMNs after metamorphosis.
384 Taken together, these data suggest that the balance between neuronal differentiation in the larva
385 and survival of neuronal precursors set aside for the adult CNS likely depends on a careful
386 balance of FGF signaling prior to metamorphosis.

387

388 **Discussion**

389 Herein, we have described the development of the *Ciona* "Neck" beyond the tailbud stage,
390 through metamorphosis and post-metamorphic neuronal differentiation. Despite reports of the
391 Neck cells being quiescent in the larva, we observe ongoing proliferation and precocious
392 ciliomotor neuron (CMN) differentiation throughout the larval stage. We also show for the first time
393 that transcription factors *Pax2/5/8.a* and *Phox2* are essential for the formation of adult (post-
394 metamorphic) CNS neurons. Through RNA sequencing we have identified the Neck
395 transcriptional program downstream of *Pax2/5/8.a,* revealing candidate target genes of
396 Pax2/5/8.a that might be important for post-metamorphic neurodevelopment. Finally, although we
397 did not identify an obvious role for either the BMP or Hedgehog pathways, we establish that Ephrin
398 and FGF signaling are responsible for patterning the Neck into differentiated and undifferentiated
399 compartments, with serious consequences for adult CNS formation if disturbed.

400 In vertebrates, *Pax2*, *Pax5* and *Pax8* are midbrain/hindbrain regulators, whereas *Phox2a*
401 and *Phox2b* regulate the development of hindbrain-derived cranial (branchiomeric) motor
402 neurons, which are also cholinergic (Curto et al., 2015; Mazzoni et al., 2013; Pattyn et al., 2000).
403 Loss of *Phox2b* ablates cranial branchial neurons and visceral motor neurons of the hindbrain in
404 mouse (Pattyn et al., 2000; Pattyn et al., 1999). Also in mouse, Phox2a promotes cranial motor
405 neuron fate over spinal cord motor neuron fate (Mazzoni et al., 2013). In *Ciona*,
406 *Pax2/5/8.a+/Phox2+* Neck cells give rise to post-metamorphic neurons that innervate pharyngeal
407 gill slits and possibly branchiomeric siphon muscles of the adult later on (Dufour et al., 2006;
408 Hozumi et al., 2015; Wada et al., 1998). In contrast, *Ciona Phox2* is not expressed in larval motor
409 neurons, which innervate (paraxial) muscles of the tail, like vertebrate spinal cord motor neurons.
410 Here we show that Pax2/5/8.a and Phox2 are required for the formation of Neck-derived
411 cholinergic CMNs in post-metamorphic *Ciona.* Taken together, these findings suggest that a
412 conserved transcriptional program for cholinergic branchiomeric efferent specification and

413 differentiation might have evolved in the last common ancestor of tunicates and vertebrates,
414 predating the origin of cranial nerves and jaw muscles.

415 Like many tunicate species, *Ciona* have a biphasic lifecycle; a motile, non-feeding larval
416 stage and a sessile, filter-feeding juvenile/adult stage. It has been traditionally assumed that the
417 larval and adult life stages are separated by a total overhaul during metamorphosis, with the adult
418 CNS completely replacing the larval CNS, thanks to quiescent neural progenitors set aside for
419 the adult nervous system (Horie et al., 2011; Hozumi et al., 2015). However, our observations
420 suggest that the larval-adult boundary might not be as sharp. Instead, we observe precocious
421 differentiation of Neck-derived CMNs that project their axons ventrally and anteriorly during the
422 late larval stage (**Figure 2J**), several hours before tail absorption and body axis rotation (Hotta et
423 al., 2020). Thus, it appears that these particular neurons are already post-mitotic and
424 differentiating during larval phase (Stage 28) and not during the post-metamorphic juvenile stage
425 as previously thought. In juveniles and adults, CMNs have been shown to use cholinergic
426 neurotransmission to regulate ciliary flow in the gill slit epithelium, which generates the water flow
427 that brings suspended food particles into the mouth (Jokura et al., 2020; Petersen et al., 1999).
428 Therefore, the early, pre-metamorphic differentiation of these neurons may be key for the rapid
429 onset of feeding behavior and further growth after metamorphosis.

430 It is unclear if the Neck also gives rise to additional neurons of the juvenile/adult. Although
431 we and others have seen Phox2+ neurons that are not innervating the gill slits (Dufour et al.,
432 2006), one cannot exclude the possibility that new Phox2+ cells arise from other compartments
433 after metamorphosis. Moreover, as the branchial sack continues to grow and form new gill slits,
434 these structures will also require neural innervation of Phox2+ cells (Dufour et al., 2006). Whether
435 this requires ongoing neurogenesis of Neck-derived Phox2+ cells or additional sources of CMN
436 progenitors is not known. One possibility is that the anteriormost cells of the Neck that activate
437 *Phox2>GFP* later in larval development might contribute to later-differentiating CMNs. It is also
438 unclear why activation of *Phox2* expression appears initially in cells that are not undergoing
439 differentiation yet (**Figure 2G**). It will be important to identify the precise function and
440 transcriptional targets of Phox2 to understand the temporal dynamics of adult neurogenesis in
441 *Ciona.*

442 In addition to post-metamorphic CMNs, the Neck also gives rise to the Neck Neuron (NN),
443 which here we show is the posteriormost cell of the Neck lineage on either side of the larva,
444 forming a bilaterally symmetric left-right pair of neurons. The NN has been previously described
445 at the early larval stage in the *C. intestinalis* whole-larva connectome studies (Ryan et al., 2016;

446 Ryan and Meinertzhagen, 2019). The function of the NN remains unknown, but the connectome
447 described it as receiving synaptic inputs from ascending MG interneuons (AMG neurons) and
448 synapsing primarily onto the basement membrane (Ryan et al., 2016). However, NNs might not
449 be fully differentiated in early larvae, and it is possible they form additional connections later in
450 larval development. Indeed, we noticed that the axon of the NN continues to extend posteriorly
451 during the swimming larval phase and can be observed exiting the trunk and entering the proximal
452 portion of the tail prior to settlement and metamorphosis. The NNs likely do not survive
453 metamorphosis as we rarely observed them in post-metamorphic juveniles. Interestingly,
454 *Pax2/5/8.a>dnFGFR* converted the entire Neck lineage into neurons that did not appear to survive
455 metamorphosis (**Figure 9B**). Because of this, we believe that the supernumerary neurons
456 generated by dnFGFR represent NN-like neurons that do not persist to the adult stage. Although
457 the supernumerary axons in the dnFGFR condition did not project towards the tail like the NNs,
458 this may be due to disrupted neuronal polarity and axon growth mechanisms. Consistent with this
459 hypothesis, we have previously observed supernumerary motor ganglion neurons aberrantly
460 project away from the tail (Stolfi et al., 2011). Future studies will be needed to identify regulatory
461 differences between CMNs and NNs and to investigate what factors determine whether a neuron
462 survives through, or perishes during, metamorphosis despite their shared lineage history. For
463 instance, it is not yet clear if sustained FGF signaling in neural progenitors is inherently pro-
464 survival, or if FGF downregulation in the Neck is simply a molecular switch for the specification of
465 NNs, which may be pre-programmed to degenerate during metamorphosis.

466 It is possible that certain post-metamorphic cell survival factors are downstream of
467 Pax2/5/8.a, including those we identified here using RNAseq approaches. One interesting
468 candidate is *Vanabin4* (*Van4*), which encodes a vanadium-binding protein and was the most
469 highly upregulated target by overexpression of Pax2/5/8.a. The biological function of vanadium
470 or vanabins has remained elusive, and it is not clear what the role of Van4 might be in the Neck
471 (Ueki et al., 2015). As adults, many tunicate species accumulate high levels of intracellular
472 vanadium, but not all species have vanabins and so their purpose remains unknown (Ueki et al.,
473 2003). One theory is that adults accumulate vanadium as a deterrent for predation (Odate and
474 Pawlik, 2007), but this alone cannot explain the high expression of vanabins in the Neck. It is
475 possible that vanadium provides a protective effect against oxidative stress (Tripathi et al., 2018),
476 which would promote or enhance survival during metamorphosis. Future studies will examine the
477 role of vanabins in *Ciona* and other marine organisms that also accumulate this transition metal
478 (Mendonca et al., 2023; Thompson et al., 2018)

Acknowledgments

We thank Shohon Rafique, Tanner Shearer, and Lindsey Cohen for technical assistance. We thank members of the lab for feedback and suggestions. We thank the Optical Microscopy Core for assistance with confocal imaging. We thank Shweta Biliya of the Molecular Evolution Core facility at Georgia Tech for processing bulk RNAseq samples. This work was supported by an NIH F32 Fellowship (F32GM150234) to EDG, an ECSEL undergraduate award to LC, an ARCS Fellowship and a Mortarboard Award to SP, and NIH award R01GM143326 and NSF IOS award 1940743 to AS.

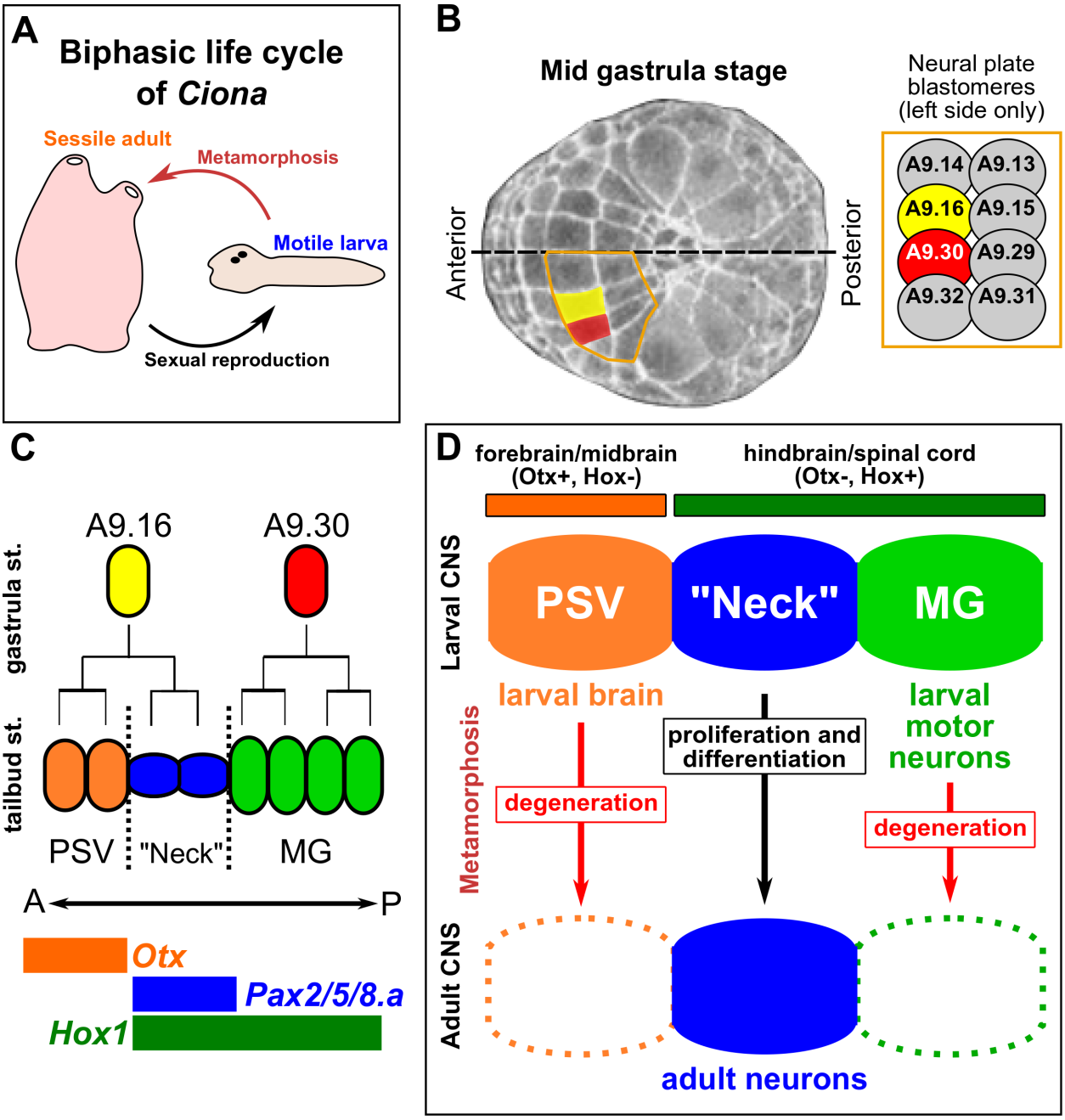

Figure 1. Specification of the "Neck" during *Ciona* embryogenesis

A) A diagram of the biphasic life cycle of *Ciona* and many other tunicates, alternating between a motile, non-feeding larva (pre-metamorphic) and a sessile, filter-feeding juvenile/adult (post-metamorphic). B) Image of mid gastrula-stage *Ciona robusta* embryo (St. 12), adapted from the Tunicanato Database (Hotta et al. 2020), with the A9.16 (yellow) and A9.30 (red) blastomeres false-colored in the neural plate. The left half of the vegetal pole-derived neural plate is outlined in orange, and blastomere identities displayed in the inset at right. Dorsal midline indicated by

512 dashed line. C) Simple diagram of the cell lineages derived from the A9.16 and A9.30 blastomeres
513 giving rise to neurons, photoreceptors, and undifferentiated precursors of the Posterior Sensory
514 Vesicle region (PSV) in orange, the “Neck” in blue, and cells of the Motor Ganglion in green.
515 Anterior(A)-Posterior(P) axis shown as left to right. Colored bars indicate expression domains of
516 conserved forebrain/midbrain regulatory gene *Otx* in orange, rhombospinal (hindbrain/spinal
517 cord) regulatory gene *Hox1* in green, and the Neck/hindbrain marker *Pax2/5/8.a* in blue. D)
518 Diagram summarizing the “traditional” view of the *Ciona* larval central nervous system (CNS),
519 indicating proposed homology of PSV, Neck, and MG compartments to vertebrate central nervous
520 system partitions, based on *Otx* and *Hox* gene expression patterns. According to this view, larval
521 neurons of the PSV/brain and MG are eliminated during metamorphosis, while the Neck
522 contributes neurons to the post-metamorphic, juvenile/adult nervous system.

523

524

525

526

527

528

529

530

531

532

533

534

535

536

537

538

Figure 2

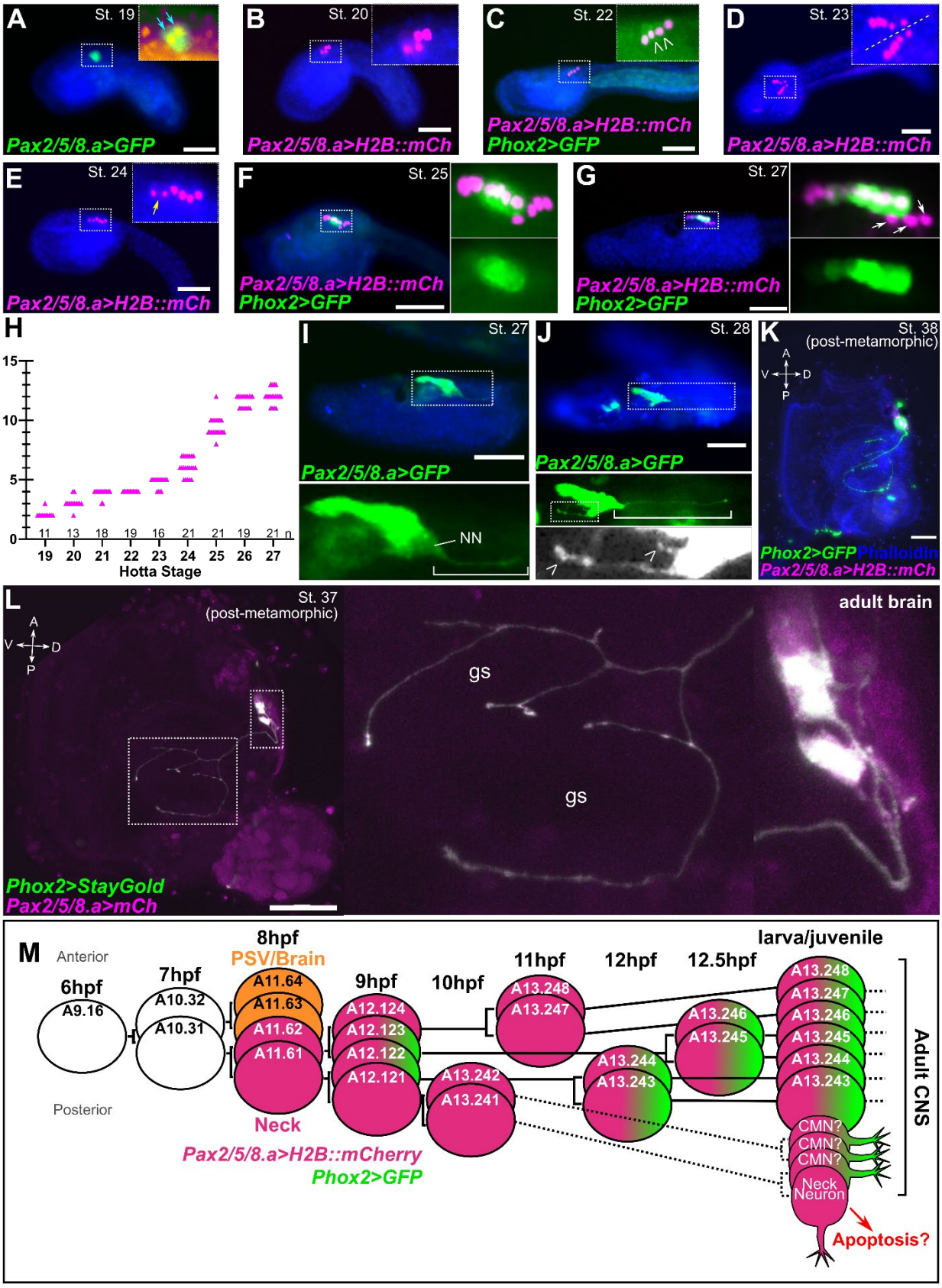
A
St. 19
Pax2/5/8.a>GFP
B
St. 20
Pax2/5/8.a>H2B::mCh
C
St. 22
Pax2/5/8.a>H2B::mCh
Phox2>GFP
D
St. 23
Pax2/5/8.a>H2B::mCh
E
St. 24
Pax2/5/8.a>H2B::mCh
F
St. 25
Pax2/5/8.a>H2B::mCh
Phox2>GFP
G
St. 27
Pax2/5/8.a>H2B::mCh
Phox2>GFP
H
# of Neck cells (per side)
Hotta Stage
11 13 18 19 16 21 21 19 21 n
19 20 21 22 23 24 25 26 27
I
St. 27
Pax2/5/8.a>GFP
NN
J
St. 28
Pax2/5/8.a>GFP
K
St. 38
(post-metamorphic)
Phox2>GFP Phalloidin
Pax2/5/8.a>H2B::mCh
L
St. 37
(post-metamorphic)
Phox2>StayGold
Pax2/5/8.a>mCh
gs
gs
adult brain
M
Anterior
Posterior
6hpf
A9.16
7hpf
A10.32
A10.31
8hpf
PSV/Brain
A11.64
A11.63
A11.62
A11.61
Neck
9hpf
A12.124
A12.123
A12.122
A12.121
10hpf
A13.242
A13.241
11hpf
A13.248
A13.247
12hpf
A13.244
A13.243
12.5hpf
A13.246
A13.245
larva/juvenile
A13.248
A13.247
A13.246
A13.245
A13.244
A13.243
CMN?
CMN?
CMN?
Neck Neuron
Adult CNS
Apoptosis?
Pax2/5/8.a>H2B::mCherry
Phox2>GFP

539

540 **Figure 2. Time-series investigation of cell division and differentiation in the Neck**

541 A-G) A time-series of images of *C. robusta* embryos electroporated with *Pax2/5/8.a* and *Phox2*
542 *(Ciona intestinalis/Type B)* reporter plasmids and fixed at different times. Approximate fixation
543 times at 20°C for each stage: St. 19: 8.75 hpf, St. 20: 9 hpf, St. 22: 10 hpf, St. 23: 11 hpf, St. 24:
544 12 hpf, St. 25: 14 hpf, St. 27: 18 hpf, St. 28: 20 hpf. Insets represent zoomed-in views of areas in
545 dashed rectangles. Nuclei counterstained with Hoechst (blue). Reporter genes used are
546 H2B::mCherry (H2B::mCh) in magenta, and Unc-76::GFP (GFP) in green. Blue arrows in (A)
547 indicating two *Pax2/5/8.a>Unc-76::GFP+* cells. Open arrowheads in (C) and (G) indicate nascent
548 *Phox2(C.intestinalis)>Unc-76::GFP* expression. Yellow arrow in (E) shows cell undergoing
549 mitosis. White arrows in (G) show differentiating neuron nuclei separating from the rest of the
550 Neck, which remains a part of the neural tube epithelium. H) Plot showing the number of
551 *Pax2/5/8.a>H2B::mCherry+* nuclei counted in embryos from each stage; n = number of embryos
552 examined per stage. I) Stage 27 larva (~18 hpf) electroporated with *Pax2/5/8.a>Unc-76::GFP,*
553 revealing differentiating Neck Neuron ("NN") extending its axon posteriorly towards the tail (white
554 bracket in inset). J) Stage 28 larva (~20 hpf) electroporated with *Pax2/5/8.a>Unc-76::GFP*
555 showing Neck Neuron axon (white bracket, middle inset) and additional axons extending ventrally
556 (open arrowheads in bottom inset), putatively representing early-differentiating post-metamorphic
557 ciliomotor neurons (CMNs). K) Stage 38 (~96 hpf) post-metamorphic juvenile showing
558 *Pax2/5/8.a>H2B::mCherry+/Phox2(C.robusta)>Unc-76::GFP+* neuronal cell bodies in the adult
559 brain (cerebral ganglion), and GFP+ axons projecting towards the gill slits. Animal counterstained
560 with phalloidin-AlexaFluor 405. See Supplemental Figure 1 for magnified view of cerebral
561 ganglion region and double-labeling with *Pax2/5/8.a>H2B::mCherry.* L) Confocal Z-stack
562 projection of a stage 37 (~72 hpf) juvenile showing *Pax2/5/8.a>Unc-76::mCherry* (magenta),
563 *Phox2(C.robusta)>Unc-76::StayGold* (green) CMNs innervating the first two gill slits (gs). Insets
564 showing higher magnification view of gill slits and brain. Merged white (green + magenta) signal
565 due to all GFP signal colocalizing with that of mCherry. A: anterior, P: posterior, D: dorsal, V:
566 ventral. M) Proposed cell lineage and cell division timing for the early Neck. Hypothesized cell
567 divisions displayed with dashed lines. Depicted expression of *Phox2* based on *Phox2>GFP*
568 reporter and not *Phox2* transcript. All scale bars = 50 µm.

569

570

571

572

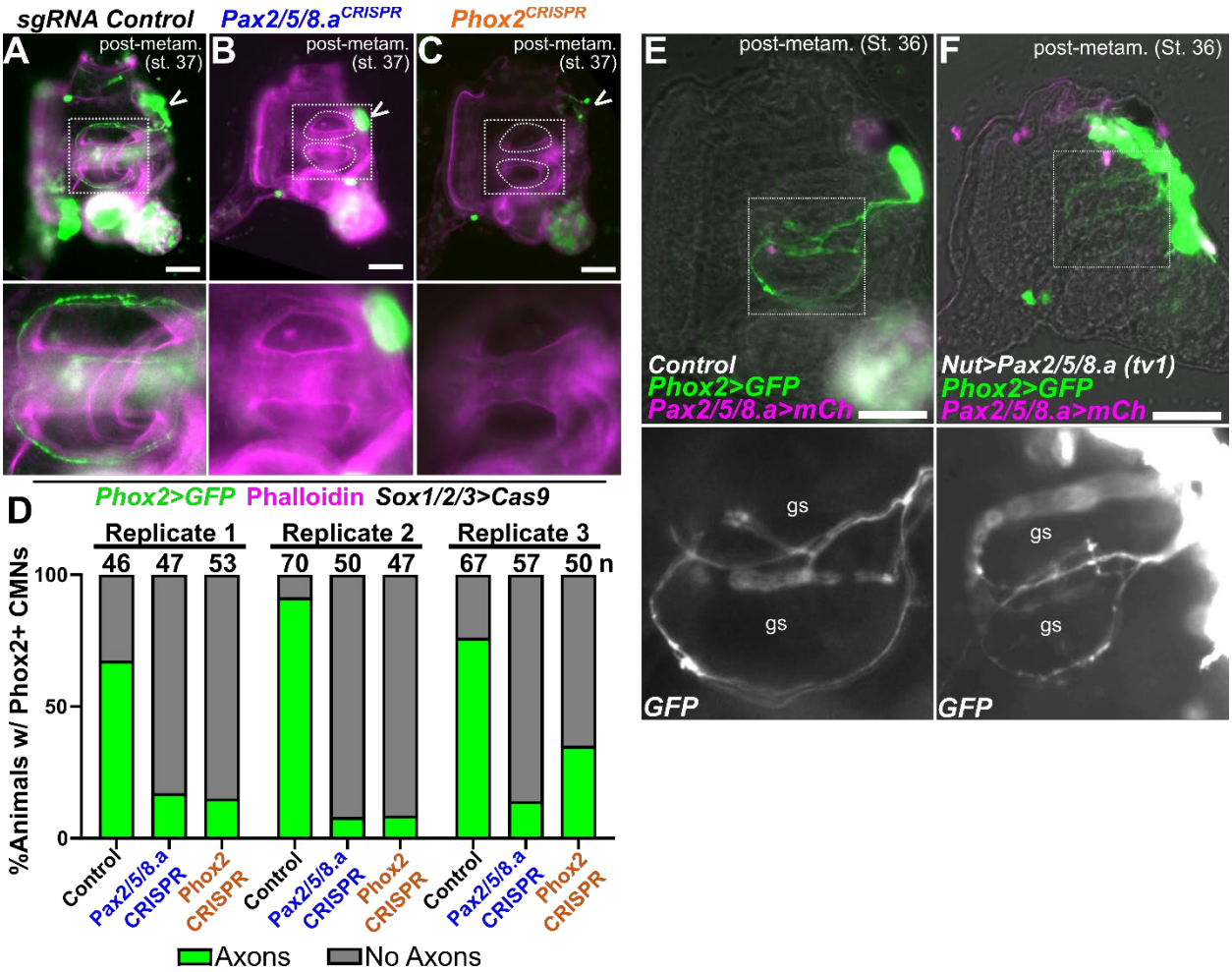

573

574 **Figure 3. Regulation of adult ciliomotor neuron specification by Pax2/5/8.a and Phox2**

575 A) "Negative control" stage 37 juvenile electroporated with *Sox1/2/3>Cas9::Geminin*$^{N\text{-}ter}$ and the
576 U6>Control sgRNA expression vector, showing normal pattern of *Phox2 (C.robusta)>Unc-*
577 *76::GFP* reporter expression in neuronal cell bodies in the brain (open arrowhead) and axons
578 innervating the gill slits (inset). B) Stage 37 juvenile in which neural-specific knockout of
579 *Pax2/5/8.a* by CRISPR/Cas9 has resulted in loss of gill slit-innervating axons (inset), suggesting
580 loss of ciliomotor neurons (CMNs). *Phox2* reporter expression in the brain (open arrowhead)
581 suggests some Phox2+ cells may still be specified. Counterstain in A-C using phalloidin-Alexa
582 Fluor 647. C) Stage 37 juvenile in which neural-specific knockout of *Phox2* has been achieved by
583 CRISPR/Cas9, also resulting in loss of CMN axons innervating the gill slits (inset), and sparse
584 Phox2+ cells remaining in the brain (open arrowhead). D) Scoring of *Phox2*+ CMN axon across
585 all three conditions represented in panels A-C, in three independent replicates (n = number of
586 individuals scored in each sample). Individuals were scored for presence or absence of

587 *Phox2>Unc-76::GFP* CMN axons innervating the gill slits. E) Stage 36 juvenile (~72 hpf) showing
588 electroporated with *Phox2(C.robusta)>Unc-76::GFP* (green) and *Pax2/5/8.a>H2B::mCherry*
589 (magenta nuclei), and a negative control *Nut>lacZ* plasmid. Inset showing gill slits (gs) innervated
590 by CMNs. H) Stage 36 juvenile electroporated with same reporters as in (F), plus *Nut>Pax2/5/8.a*
591 *(tv1)* to drive expression of Pax2/5/8.a in the entire larval neural tube. *Phox2* reporter is expanded
592 in the resulting juveniles, though there is no noticeable increase in CMN axons innervating the gill
593 slits (gs, inset). All scale bars = 50 µm.

594

595

596

597

598

599

600

601

602

603

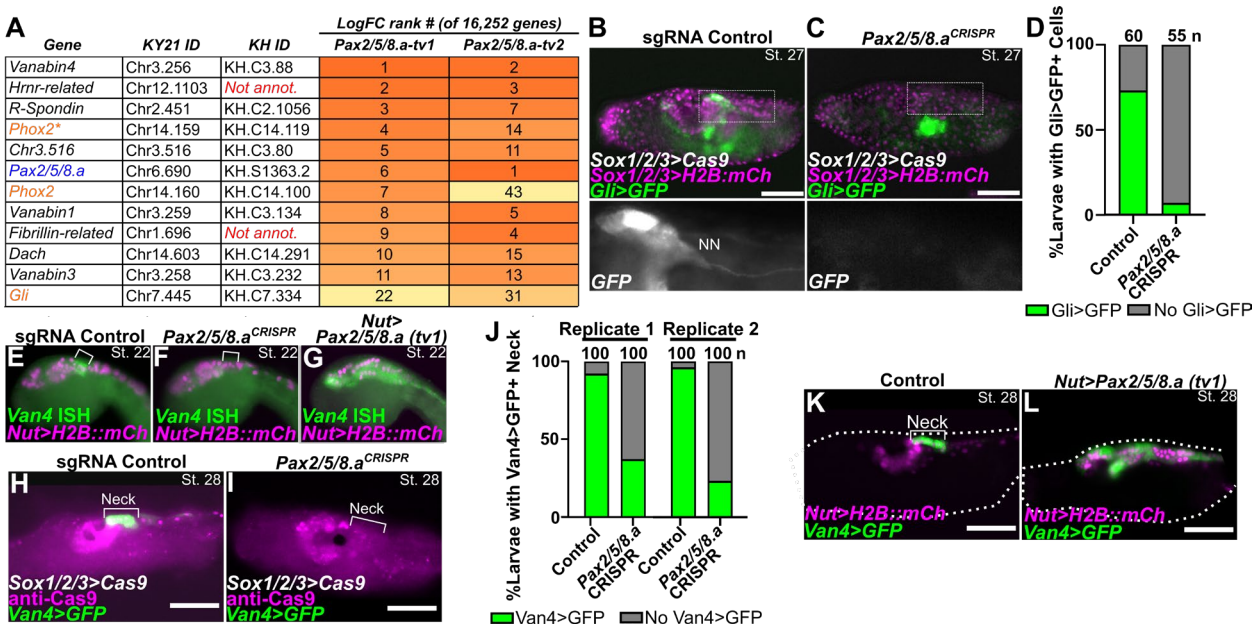

Gene	KY21 ID	KH ID	LogFC rank # (of 16,252 genes) Pax2/5/8.a-tv1	Pax2/5/8.a-tv2
Vanabin4	Chr3.256	KH.C3.88	1	2
Hrnr-related	Chr12.1103	*Not annot.*	2	3
R-Spondin	Chr2.451	KH.C2.1056	3	7
*Phox2**	Chr14.159	KH.C14.119	4	14
Chr3.516	Chr3.516	KH.C3.80	5	11
Pax2/5/8.a	Chr6.690	KH.S1363.2	6	1
Phox2	Chr14.160	KH.C14.100	7	43
Vanabin1	Chr3.259	KH.C3.134	8	5
Fibrillin-related	Chr1.696	*Not annot.*	9	4
Dach	Chr14.603	KH.C14.291	10	15
Vanabin3	Chr3.258	KH.C3.232	11	13
Gli	Chr7.445	KH.C7.334	22	31

Figure 4. Identifying a Neck-specific gene expression downstream of Pax2/5/8.a

A) Table of rank ordered genes upregulated by Pax2/5/8.a overexpression in *Ciona* embryos compared to negative control, as measured by bulk RNAseq. LogFC rank # = ranking of gene when sorting all genes by average Log2 fold-change between the negative control condition (*Nut>lacZ)* and overexpression conditions (*Nut>Pax2/5/8.a, tv1 or tv2).* See text for details. Kyoto 2021 (KY21) and KyotoHoya (KH) gene identification numbers are given for each gene. Genes in orange font are previously known Pax2/5/8.a targets, identified by morpholino knockdown (Imai et al., 2009). Asterisk denotes C-terminal fragment gene model of *Phox2* (see text for details). Differential expression of 16,252 gene models was analyzed in total. B) Negative control animal showing *Gli>Unc76:GFP (Gli>GFP; green)* reporter gene expression in the Neck and Neck neuron (NN). C) CRISPR/Cas9-mediated mutagenesis of *Pax2/5/8.a* results in loss of *Gli>GFP* reporter gene expression in the Neck. *Sox1/2/3* promoter was used to drive expression of Cas9::Geminin$^{N\text{-}ter}$ and H2B::mCherry (magenta nuclei) in the ectoderm, including the nervous system. D) Scoring of *Gli+* Neck cells for samples represented in panels B and C. Individuals were scored for presence or absence of *Gli>GFP* cells in the Neck region, posterior to the ocellus and otolith. E) *In situ* mRNA hybridization for Pax2/5/8.a downstream gene *Vanabin4 (Van4)* in negative control embryo (left), showing specific expression in the Neck (bracket) at Stage 22 (10hpf). F) *Pax2/5/8.a* knockout by CRISPR/Cas9 in the nervous system (using *Sox1/2/3>Cas9)* results in loss of *Van4* mRNA *in situ* signal in the Neck. G) Overexpression of *Pax2/5/8.a (transcript variant 1)* in throughout the neural tube (*Nut>Pax2/5/8.a tv1)* results in widespread, ectopic expression of *Van4*, confirming this gene as being downstream of Pax2/5/8.a as indicated

626 by RNAseq. All embryos electroporated with *Nut>H2B::mCherry* (magenta nuclei). (H)
627 *Van4>Unc-76::GFP* reporter expression (green) also specifically labels the Neck (bracket) in
628 Stage 28 negative control larvae (~20 hpf). I) Knockout of *Pax2/5/8.a* in the nervous system
629 results in loss of *Van4* reporter expression. Cas9 protein visualized by immunostaining (magenta).
630 J) Scoring of *Van4>Unc-76::GFP* reporter expression in *Pax2/5/8.a* CRISPR larvae represented
631 in H and I, showing dramatic reduction in frequency of *Van4+* larvae in *Pax2/5/8.a* CRISPR larvae
632 compared to negative control larvae, in two independent replicates. K) Stage 28 larva
633 electroporated with *Nut>H2B::mCherry* (magenta nuclei), *Van4>Unc-76::GFP* (green) reporters,
634 and *Nut>LacZ* control. L) Larva electroporated with same reporters as in (K), together with
635 *Nut>Pax2/5/8.a tv1,* showing expansion of *Van4* reporter expression throughout the neural tube.
636 In D and J, n = number of individuals scored in each sample. All scale bars = 50 µm.

637

638

639

640

641

642

643

644

645

646

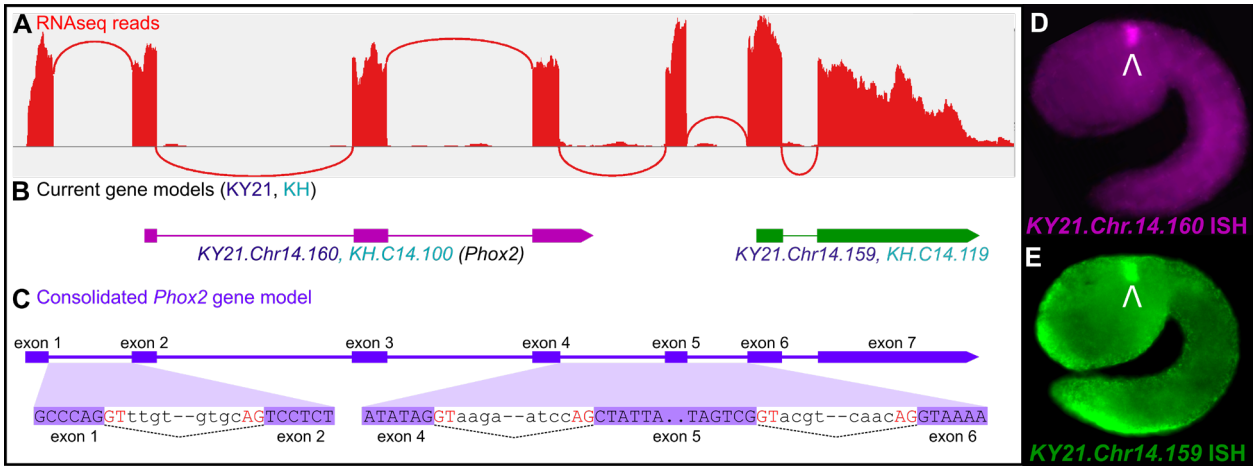

Figure 5. RNAseq reveals cryptic exons in an updated *Phox2* gene model

A) "Sashimi" plot of RNASeq reads mapped to the *Phox2* locus in the *C. robusta* genome in (adapted from IGV). Red lines indicate reads spanning exon-exon junctions. B) Current Kyoto 2021 (KY21) and KyotoHoya (KH) gene models. Comparison to RNAseq reads in (A) shows that KY21.Chr14.160/KH.C14.100 and KY21.Chr14.159/KH.C14.119 should be consolidated into a single gene models, and reveals the existence of cryptic exons 1 and 5, which are not represented in any current *Ciona* gene model. C) Updated, correct *Phox2* gene model confirmed by cDNA cloning (**Supplemental Figure 3A**), showing splice donor (GT) and splice acceptor (AG) sequences flanking newly identified exonic and intronic sequences. D-E) *In situ* mRNA hybridization using probes designed for *Phox2* (D) or *Chr14.159* (E) current gene model shows identical expression pattern in the Neck at stage 22 (~10 hpf), further suggesting the two gene models are likely to represent a single *Phox2* transcript.

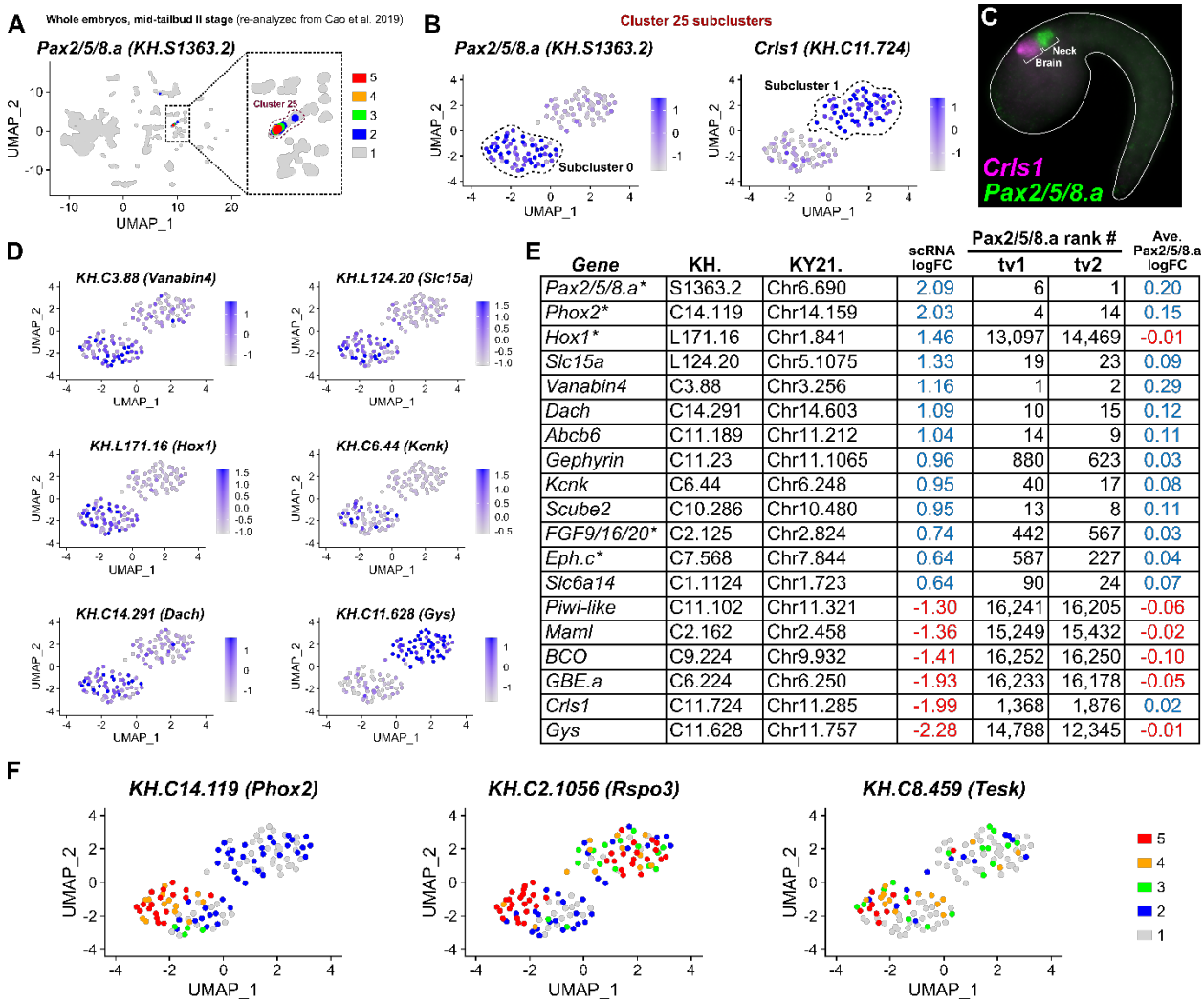

E

Gene	KH.	KY21.	scRNA logFC	Pax2/5/8.a rank # tv1	Pax2/5/8.a rank # tv2	Ave. Pax2/5/8.a logFC
*Pax2/5/8.a**	S1363.2	Chr6.690	2.09	6	1	0.20
*Phox2**	C14.119	Chr14.159	2.03	4	14	0.15
*Hox1**	L171.16	Chr1.841	1.46	13,097	14,469	-0.01
Slc15a	L124.20	Chr5.1075	1.33	19	23	0.09
Vanabin4	C3.88	Chr3.256	1.16	1	2	0.29
Dach	C14.291	Chr14.603	1.09	10	15	0.12
Abcb6	C11.189	Chr11.212	1.04	14	9	0.11
Gephyrin	C11.23	Chr11.1065	0.96	880	623	0.03
Kcnk	C6.44	Chr6.248	0.95	40	17	0.08
Scube2	C10.286	Chr10.480	0.95	13	8	0.11
*FGF9/16/20**	C2.125	Chr2.824	0.74	442	567	0.03
*Eph.c**	C7.568	Chr7.844	0.64	587	227	0.04
Slc6a14	C1.1124	Chr1.723	0.64	90	24	0.07
Piwi-like	C11.102	Chr11.321	-1.30	16,241	16,205	-0.06
Maml	C2.162	Chr2.458	-1.36	15,249	15,432	-0.02
BCO	C9.224	Chr9.932	-1.41	16,252	16,250	-0.10
GBE.a	C6.224	Chr6.250	-1.93	16,233	16,178	-0.05
Crls1	C11.724	Chr11.285	-1.99	1,368	1,876	0.02
Gys	C11.628	Chr11.757	-2.28	14,788	12,345	-0.01

Figure 6. Analyzing Neck-specific gene expression in single-cell RNAseq data.

A) Re-analysis of published whole-embryo *C. robusta* single-cell RNA sequencing (scRNAseq) data from Cao et al. (2019) (Cao et al., 2019) revealed a cluster of cells (Cluster 25) enriched for Neck marker *Pax2/5/8.a* (magnified view of boxed area in inset). Differential gene expression "FeaturePlot" color-coded as measured by "RNA" assay in Seurat. B) Differential gene expression as measured by "integrated" assay of reclustered cells from Cluster 25 showing enrichment of *Pax2/5/8.a* reads in Subcluster "0" relative to subcluster "1", and enrichment of *Crls1* in subcluster "1" relative to subcluster "0". C) Two-color double mRNA *in situ* hybridization for *Crls1* (magenta) and *Pax2/5/8.a* (green) in a Stage-22 embryo confirm that subcluster "0" represents the Neck and subcluster "1" represents brain/posterior sensory vesicle cells just anterior to the Neck. D) Differential gene expression FeaturePlots showing enrichment of various genes in the Neck (subcluster 0) relative to the brain (subcluster 1), or vice-versa (e.g. *Glycogen synthase, or Gys).*

680 All plots generated by “integrated” assay in Seurat. E) Table of genes comparing enrichment (blue
681 font) or depletion (red font) in subcluster “0” cells to upregulation upon overexpression of
682 *Pax2/5/8.a* transcript variants 1 and 2. “Ave. Pax2/5/8/a logFC” = average tv1 and tv2 logFC
683 values as compared to a negative control. Asterisks denote previously known Neck marker genes.
684 *Hox1* is a rare exception of a gene that is enriched in the Neck by scRNAseq but is not upregulated
685 by Pax2/5/8.a. F) Differential gene expression FeaturePlots (5-color scale, “integrated” assay)
686 showing higher expression of *Phox2, Rspo3,* and *Tesk* in roughly half of subcluster 0,
687 recapitulating the distinction between *Phox2+* middle cells and flanking Phox2-negative cells seen
688 by reporter assays (Figure 2).

689

690

691

692

693

694

695

696

697

698

699

700

701

702

703

704

705

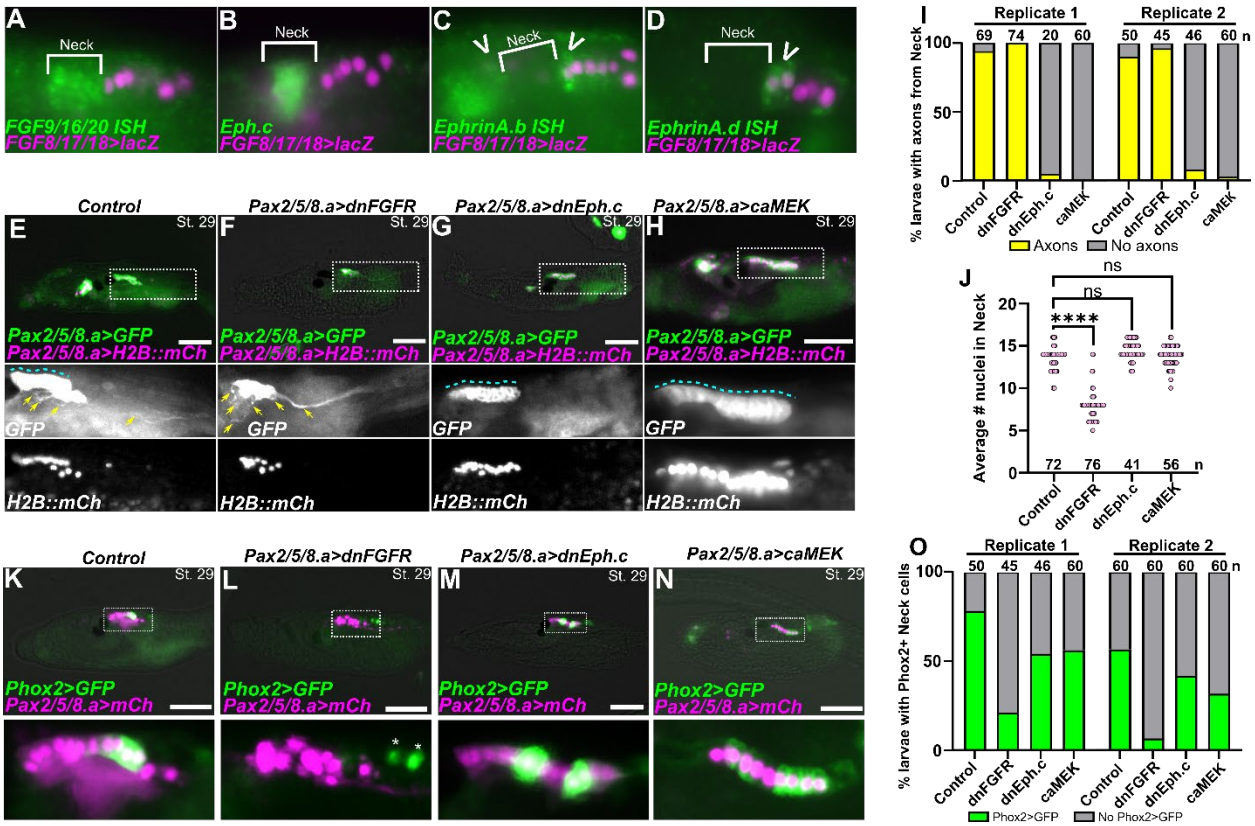

Figure 7. Ephrin/Eph and FGF/MEK signaling pathways regulate differentiation in the Neck

A) *In situ* hybridization (ISH) for *FGF9/16/20* (green), showing expression in the Neck at stage 22. B) ISH for *Eph.c* (green), showing expression in the Neck (St. 22), more strongly in middle cells. C) ISH for *EphrinA.b* (green), showing expression in the anterior cells of the A9.30 lineage as well as the brain region (open arrowhead), both abutting the limits of the Neck. D) ISH for *EphrinA.d* (green), showing expression in the anterior cells of the A9.30 lineage (open arrowhead). In panels A-D, neighboring A9.30 lineage is marked by *FGF8/17/18>LacZ,* revealed by β–galactosidase immunostaining (magenta nuclei). E) Negative control Stage 29 larva (~21 hpf) electroporated with *Pax2/5/8.a>LacZ* control, *Pax2/5/8.a>Unc-76::GFP* (green), and *Pax2/5/8.a>H2B::mCherry* (magenta nuclei) showing the Neck giving rise to both undifferentiated cells forming an epithelium in the neural tube (blue dashed line) as well as differentiating neurons and extending axons (yellow arrows). F) Larva electroporated with *Pax2/5/8.a>dnFGFR,* showing loss of epithelial structure in the Neck and supernumerary *Pax2/5/8.a+* axons. G) Larva electroporated with *Pax2/5/8.a>dnEph.c,* showing expansion of the the undifferentiated neuroepithelium and loss of axons emanating from the Neck. H) Larva electroporated with *Pax2/5/8.a>caMEK,* which also expanded the neuroepithelial state and suppressed neuronal differentiation and axon growth. I) Scoring of larvae represented in panels E-H, showing almost

complete loss of Neck-derived axons in larvae expressing dnEph.c or caMEK in the Neck, across two replicates. J) Plot showing average number of *Pax2/5/8+* nuclei counted in larvae represented in panels E-H, showing significantly fewer nuclei in the dnFGFR condition. K) Negative control larva electroporated with *Pax2/5/8.a>LacZ* control, with *Pax2/5/8.a>Unc76:mCh* and *Pax2/5/8.a>H2b:mCh* (labeled as *Pax2/5/8.a>mCh),* showing *Phox2(C.robusta)>Unc-76::GFP* expression in a subset of Neck cells (green). L) Overexpression of dnFGFR in the Neck abolished *Phox2>GFP* reporter expression. M) Overexpression of dnEph.c expands *Phox2* expression in a variable manner. N) caMEK overexpression is similar to that of dnEph.c, resulting in variable expansion of *Phox2* reporter expression. O) *Phox2>Unc-76::GFP* expression was scored in larvae represented in panels K-N, across two independent replicates. While dnFGFR results in loss of *Phox2* reporter expression, dnEph.c and caMEK do not. In panels I, J, and O, n = number of individuals scored in each sample. All scale bars = 50 µm.

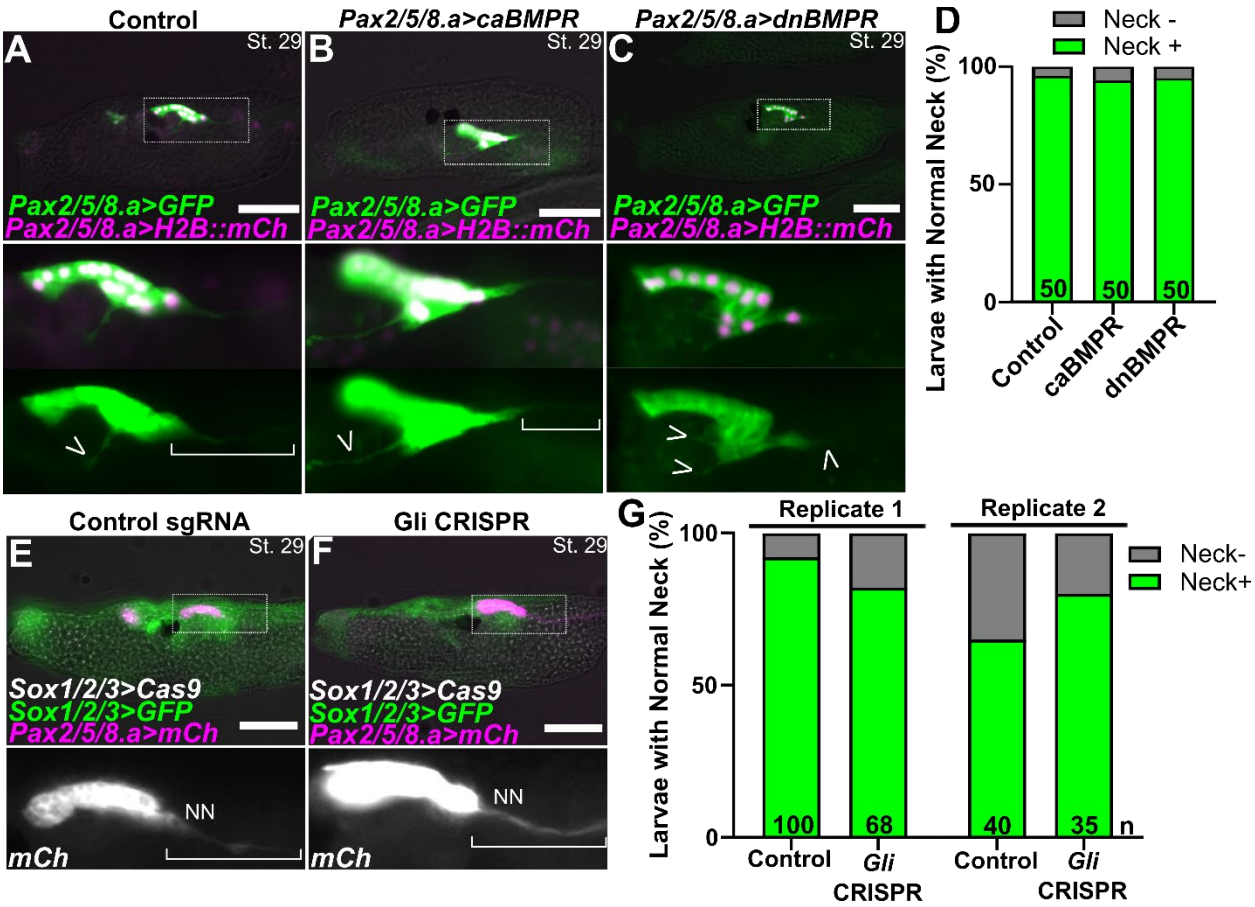

Figure 8. BMP and Hedgehog signaling do not affect differentiation and morphogenesis in the Neck

A) Negative control larva electroporated with *Pax2/5/8.a>lacZ, Pax2/5/8.a>Unc76::GFP* (*Pax2/5/8.a>GFP;* green)*, and Pax2/5/8.a>H2B:mCh* (magenta) showing typical morphology of the Neck, with some neuroepithelial cells anteriorly and differentiating neurons and axons (bracket, open arrowhead) in the posterior. B) Larva expressing a constitutively-active BMP receptor (caBMPR), showing no noticeable difference in Neck-derived axons (bracket and open arrowhead). C) Larva expressing a dominant-negative BMP receptor (dnBMPR), also showing no noticeable effect on Neck morphogenesis or patterning. D) Scoring for "typical" Neck morphology in larvae represented in panels A-C. E) Negative CRISPR control larva expressing *Sox1/2/3>Cas9:Geminin$^{N\text{-}ter}$* and *Sox1/2/3>Unc76::GFP* (*Sox1/2/3>GFP*, green) reporter, with *Pax2/5/8.a>Unc-76::mCherry* (*Pax2/5/8.a>mCh*; magenta) labeling the Neck including the axon of the Neck neuron. F) Knocking out the Hedgehog effector-encoding gene *Gli* also does not alter Neck morphogenesis. G) Scoring of larvae represented in E and F. In panels D and G, n = number of individuals scored in each sample. All scale bars = 50 µm.

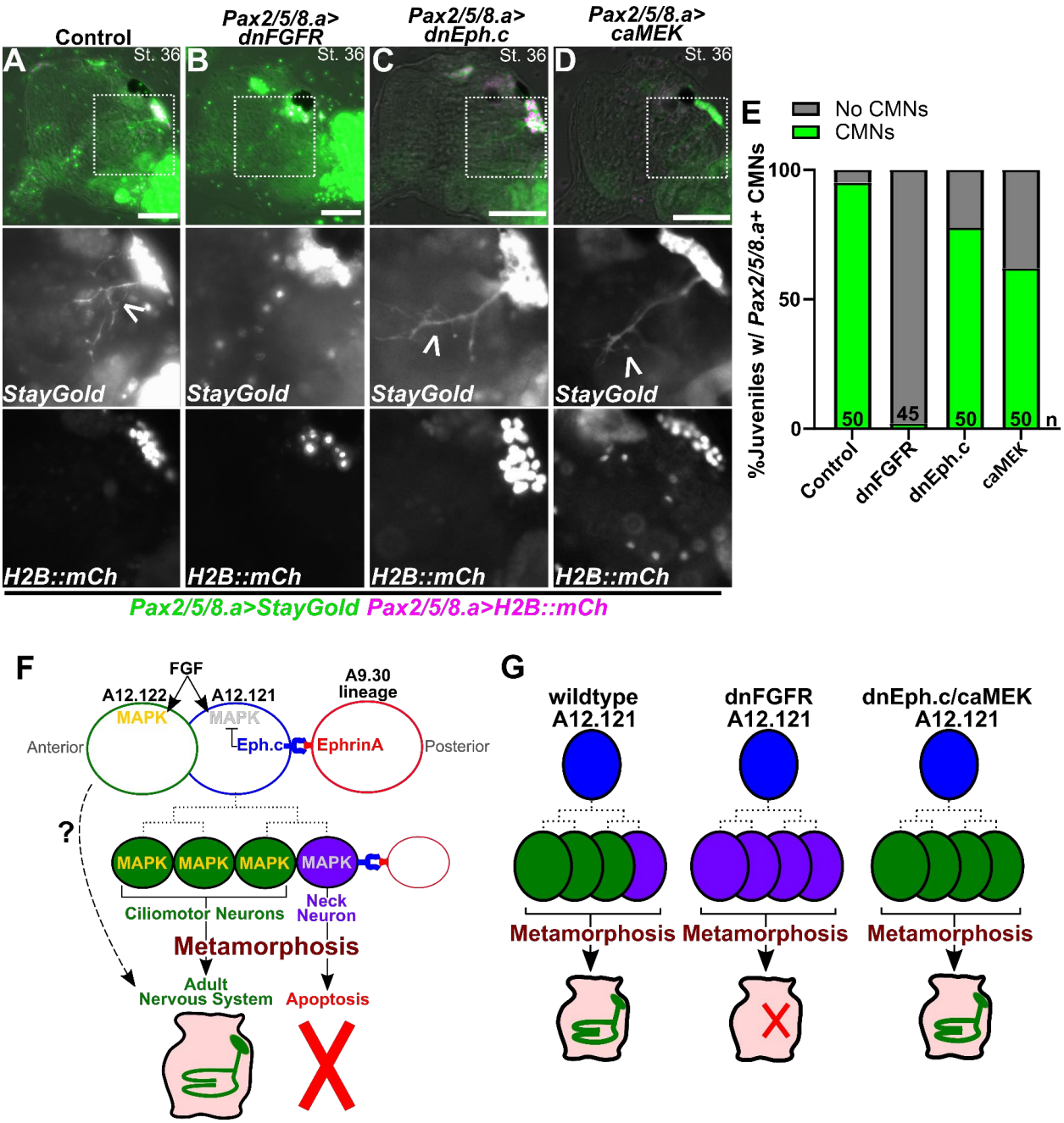

Figure 9. FGF signaling is required for survival of CMN precursors through metamorphosis

A-D) Stage 36 juveniles (~72 hpf) electroporated with *Pax2/5/8.a>Unc-76::StayGold* (*Pax2/5/8.a>StayGold*; green) and *Pax2/5/8.a>H2B::mCherry* (magenta), showing growing ciliomotor (CMN) axons (open arrowhead) in the process of innervating the gill slits. A) Negative controls expressing *Pax2/5/8.a>LacZ* show normal CMNs. B) *Pax2/5/8.a>dnFGFR* eliminates CMN axons, suggesting maintenance of FGF/MAPK signaling is important for specification of CMNs and survival through metamorphosis. C) Juveniles expressing dnEph.c still give rise to

775 CMNs (open arrowhead) during metamorphosis, indicating an ability to recover from earlier
776 suppression of differentiation in the larva (see Figure 7). D) Juvenile expressing caMEK also
777 recover, growing CMN axons (open arrowhead) during metamorphosis. E) Scoring of juveniles
778 represented by panels A-D, showing near total loss of CMNs in juveniles derived from larvae
779 expressing dnFGFR in the Neck. F) Diagram explaining model for Ephrin/Eph-mediated
780 suppression of FGF/MAPK signaling in the the posteriormost cell of the Neck, which becomes the
781 Neck Neuron, and hypothesized cell lineage from A12.121 (dashed lines). More anterior cells
782 escape Ephrin signaling at different times, giving rise to precursors of the adult nervous system
783 including CMNs, while the Neck Neuron does not appear to survive metamorphosis. The
784 uncertain contribution of A12.122 derivatives to the adult nervous system indicated by dashed
785 arrow. G) Diagram explaining the different manipulations tested and their effects on CMN
786 formation in juveniles. In wildtype animals, the Neck Neuron (lavender) does not survive
787 metamorphosis, and more anterior CMN precursors differentiate during late larval/early juvenile
788 stages. In *Pax2/5/8.a>dnFGFR*-electroporated animals, the entire Neck is converted to Neck
789 Neuron-like neurons, which are all eliminated during metamorphosis. In individuals electoporated
790 with *Pax2/5/8.a>dnEph.c* or *Pax2/5/8.a>caMEK,* sustained FGF signaling temporarily suppresses
791 neuronal differentiation in the Neck during larval stages, but the cells eventually “recover” during
792 metamorphosis to give rise to CMNs.

793

794

795

796

797

798

799

800

801

802

803

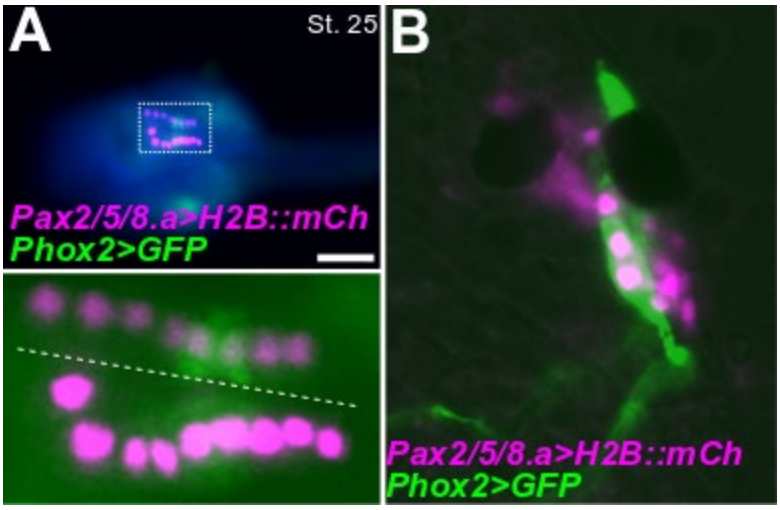

Supplemental Figure 1.

A) A Stage 25 (~14 hpf) embryo expressing *Pax2/5/8.a>H2B::mCherry* (magenta) and *Phox2(C.intestinalis)>Unc76::GFP* (green). The Neck on the left of the midline (dashed line) has nine Pax2/5/8.a+ nuclei compared to only eight on the right side, demonstrating that Neck cell divisions can vary between left/right sides within an individual. Scale bar is 50 μm. B) Close up of post-metamorphic Stage 38 (~96 hpf) juvenile brain shows Pax2/5/8.a>H2B:mCherry+ nuclei (magenta) Phox2(*C.robusta*)>Unc76:GFP+ neurons (green) innervating the gill slits. Individual is the same as in **Figure 1K**.

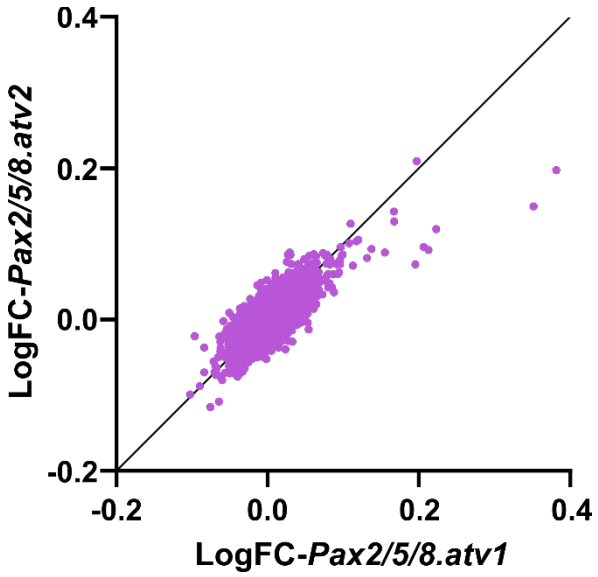

Supplemental Figure 2.

Dot plot matrix showing comparison between average Log2 fold-change values for all 16,252 genes upon overexpression of Pax2/5/8.a transcript variant 1 (tv1) and 2 (tv2). Raw data can be found in **Supplemental Table 1**.

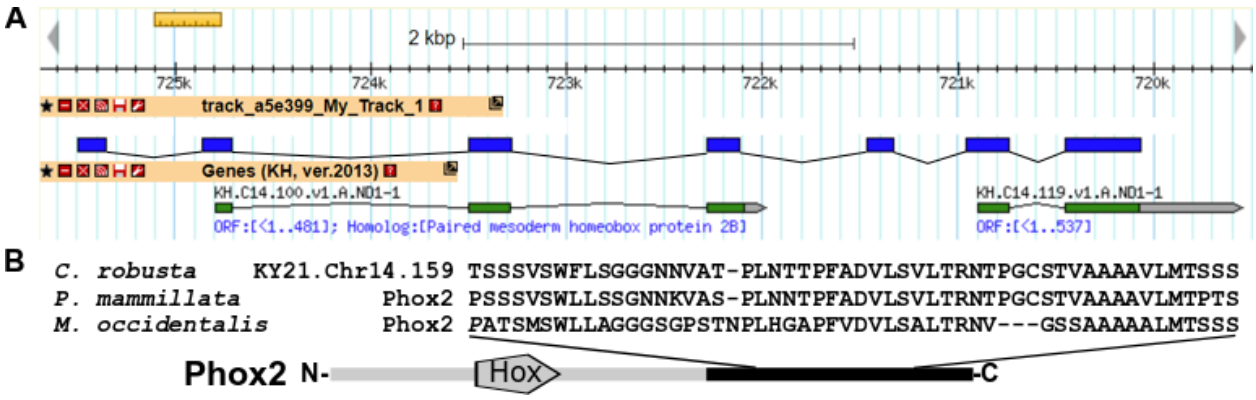

Supplemental Figure 3.

A) Alignment of *Phox2* cDNA sequence (blue) to the KyotoHoya (KH) *Ciona robusta* (*intestinalis* type A) genome (green). The sequence reveals a cryptic exon 1 and 5 of Phox2, linking gene models KH.C14.100 and KH.C14.119. Panel adapted from KH genome browser (Satou et al., 2005). B) Alignment of proposed Phox2 C-terminus amino acid sequence and Phox2 protein sequences from *Phallusia mammillata* (*Phmamm.g00000831*) and *Molgula occidentalis* (*Moocci.g00011046*)(Brozovic et al., 2018).

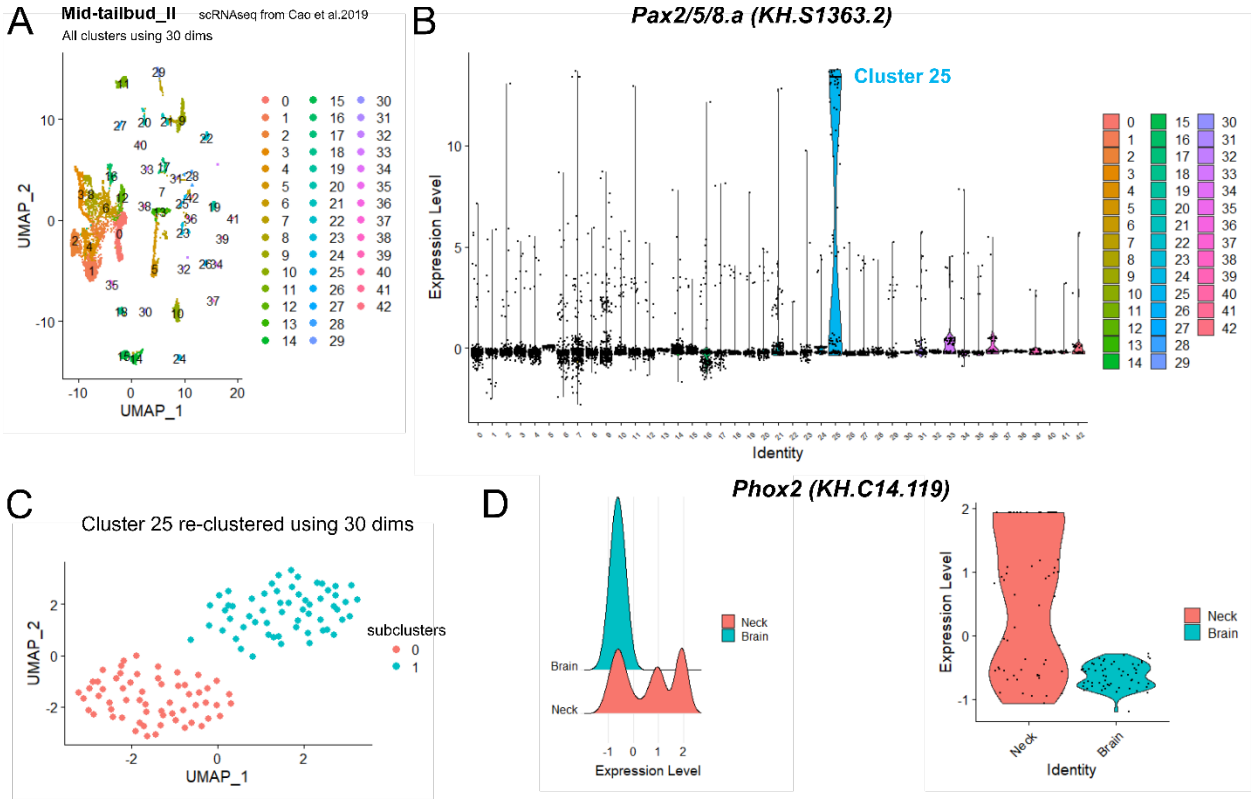

Supplemental Figure 4.

A) Clustering of re-analyzed scRNAseq data from Mid-tailbud II stage (Cao et al., 2019). B) Cluster 25 shows enriched expression *Pax2/5/8.a*. C) Re-clustering of cells only in Cluster 25 revealed subcluster “0” (Neck) and subcluster “1” (brain) showing clear separation. D) Phox2 expression is further enriched in a specific subset of subcluster 0 cells, as indicated by both ridge (left) and violin (right) plots, mirroring the detection of *Phox2>GFP* reporter expression in only a subset of Neck cells during embryonic stages.

Supplemental Figure 5

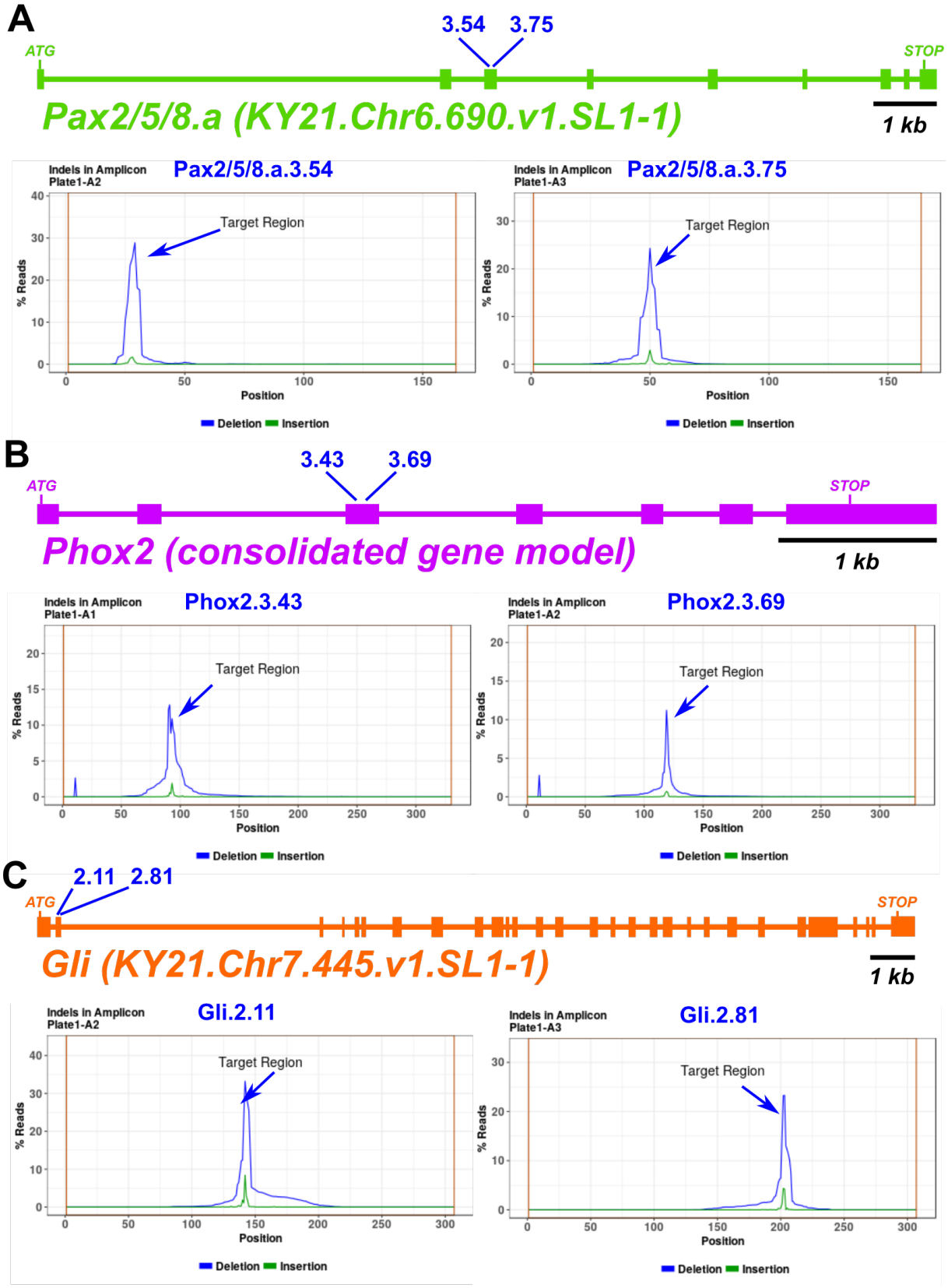

854 **Supplemental Figure 5.**

855 Indel plots generated by Amplicon-EZ Next Generation Sequencing from Azenta/Genewiz for
856 validation of sgRNAs targeting (A) *Pax2/5/8.a*, (B) *Phox2* and, (C) *Gli*.

857

858 **Supplemental Table 1. Differential gene expression in Pax2/5/8.a overexpression**
859 **conditions as measured by bulk RNAseq.**

860

861 **Supplemental Table 2. Transcripts enriched or depleted in Cluster 25 of mid-tailbud II**
862 **scRNAseq re-analysis.**

863

864 **Supplemental Table 3. Transcripts enriched or depleted in subcluster 0 (Neck) vs.**
865 **subcluster 1 (larval brain) within Cluster 25 of mid-tailbud II scRNAseq re-analysis.**

866

867 **Supplemental Table 4. Cross-referencing subcluster 0 scRNAseq differential gene**
868 **expression and Log2 fold-change from Pax2/5/8.a overexpression bulk RNAseq.**

869

870 **Supplemental Video 1. 3D projection of CMNs in post-metamorphic juvenile shown in**
871 **Figure 2L.**

872

873

874

875

876

877

878

879

880 **References**

881 Abitua, P.B., Gainous, T.B., Kaczmarczyk, A.N., Winchell, C.J., Hudson, C., Kamata, K., Nakagawa, M.,
882 Tsuda, M., Kusakabe, T.G., Levine, M., 2015. The pre-vertebrate origins of neurogenic placodes. Nature
883 524, 462-465.
884 Beh, J., Shi, W., Levine, M., Davidson, B., Christiaen, L., 2007. FoxF is essential for FGF-induced migration
885 of heart progenitor cells in the ascidian Ciona intestinalis.
886 Bernadskaya, Y., Christiaen, L., 2016. Transcriptional control of developmental cell behaviors. Annual
887 review of cell and developmental biology 32, 77-101.
888 Brozovic, M., Dantec, C., Dardaillon, J., Dauga, D., Faure, E., Gineste, M., Louis, A., Naville, M., Nitta, K.R.,
889 Piette, J., 2018. ANISEED 2017: extending the integrated ascidian database to the exploration and
890 evolutionary comparison of genome-scale datasets. Nucleic acids research 46, D718-D725.
891 Cao, C., Lemaire, L.A., Wang, W., Yoon, P.H., Choi, Y.A., Parsons, L.R., Matese, J.C., Wang, W., Levine, M.,
892 Chen, K., 2019. Comprehensive single-cell transcriptome lineages of a proto-vertebrate. Nature 571,
893 349-354.
894 Christiaen, L., Burighel, P., Smith, W.C., Vernier, P., Bourrat, F., Joly, J.-S., 2002. Pitx genes in Tunicates
895 provide new molecular insight into the evolutionary origin of pituitary. Gene 287, 107-113.
896 Christiaen, L., Wagner, E., Shi, W., Levine, M., 2009a. Electroporation of transgenic DNAs in the sea
897 squirt Ciona. Cold Spring Harbor Protocols 2009, pdb. prot5345.
898 Christiaen, L., Wagner, E., Shi, W., Levine, M., 2009b. Isolation of sea squirt (Ciona) gametes,
899 fertilization, dechorionation, and development. Cold Spring Harbor Protocols 2009, pdb. prot5344.
900 Community, T.G., 2022. The Galaxy platform for accessible, reproducible and collaborative biomedical
901 analyses: 2022 update. Nucleic Acids Research 50, W345-W351.
902 Conklin, E.G., 1905. The organization and cell-lineage of the ascidian egg. Academy of Natural Sciences.
903 Curto, G.G., Gard, C., Ribes, V., 2015. Structures and properties of PAX linked regulatory networks
904 architecting and pacing the emergence of neuronal diversity, Seminars in cell & developmental biology.
905 Elsevier, pp. 75-86.
906 Davidson, B., Shi, W., Beh, J., Christiaen, L., Levine, M., 2006. FGF signaling delineates the cardiac
907 progenitor field in the simple chordate, Ciona intestinalis. Genes & development 20, 2728-2738.
908 Delsuc, F., Brinkmann, H., Chourrout, D., Philippe, H., 2006. Tunicates and not cephalochordates are the
909 closest living relatives of vertebrates. Nature 439, 965-968.
910 Di Gregorio, A., 2020. The notochord gene regulatory network in chordate evolution: Conservation and
911 divergence from Ciona to vertebrates. Current Topics in Developmental Biology 139, 325-374.
912 Dufour, H.D., Chettouh, Z., Deyts, C., De Rosa, R., Goridis, C., Joly, J.-S., Brunet, J.-F., 2006. Precraniate
913 origin of cranial motoneurons. Proceedings of the National Academy of Sciences 103, 8727-8732.
914 Dynes, J.L., Ngai, J., 1998. Pathfinding of olfactory neuron axons to stereotyped glomerular targets
915 revealed by dynamic imaging in living zebrafish embryos. Neuron 20, 1081-1091.
916 Farley, E.K., Olson, K.M., Zhang, W., Brandt, A.J., Rokhsar, D.S., Levine, M.S., 2015. Suboptimization of
917 developmental enhancers. Science 350, 325-328.
918 Fodor, A., Liu, J., Turner, L., Swalla, B.J., 2021. Transitional chordates and vertebrate origins: Tunicates.
919 Current Topics in Developmental Biology 141, 149-171.
920 Gandhi, S., Razy-Krajka, F., Christiaen, L., Stolfi, A., 2018. CRISPR knockouts in ciona embryos. Transgenic
921 Ascidians, 141-152.
922 Guignard, L., Fiúza, U.-M., Leggio, B., Laussu, J., Faure, E., Michelin, G., Biasuz, K., Hufnagel, L.,
923 Malandain, G., Godin, C., 2020. Contact area–dependent cell communication and the morphological
924 invariance of ascidian embryogenesis. Science 369, eaar5663.

Haeussler, M., Schönig, K., Eckert, H., Eschstruth, A., Mianné, J., Renaud, J.-B., Schneider-Maunoury, S., Shkumatava, A., Teboul, L., Kent, J., 2016. Evaluation of off-target and on-target scoring algorithms and integration into the guide RNA selection tool CRISPOR. Genome biology 17, 1-12.
Hafemeister, C., Satija, R., 2019. Normalization and variance stabilization of single-cell RNA-seq data using regularized negative binomial regression. Genome biology 20, 296.
Haupaix, N., Stolfi, A., Sirour, C., Picco, V., Levine, M., Christiaen, L., Yasuo, H., 2013. p120RasGAP mediates ephrin/Eph-dependent attenuation of FGF/ERK signals during cell fate specification in ascidian embryos. Development 140, 4347-4352.
Hirano, M., Ando, R., Shimozono, S., Sugiyama, M., Takeda, N., Kurokawa, H., Deguchi, R., Endo, K., Haga, K., Takai-Todaka, R., 2022. A highly photostable and bright green fluorescent protein. Nature Biotechnology 40, 1132-1142.
Horie, T., Shinki, R., Ogura, Y., Kusakabe, T.G., Satoh, N., Sasakura, Y., 2011. Ependymal cells of chordate larvae are stem-like cells that form the adult nervous system. Nature 469, 525-528.
Hotta, K., Dauga, D., Manni, L., 2020. The ontology of the anatomy and development of the solitary ascidian Ciona: the swimming larva and its metamorphosis. Scientific reports 10, 1-16.
Hozumi, A., Horie, T., Sasakura, Y., 2015. Neuronal map reveals the highly regionalized pattern of the juvenile central nervous system of the ascidian Ciona intestinalis. Developmental Dynamics 244, 1375-1393.
Hudson, C., Yasuo, H., 2021. Neuromesodermal lineage contribution to CNS development in invertebrate and vertebrate chordates. Genes 12, 592.
Ikuta, T., Saiga, H., 2007. Dynamic change in the expression of developmental genes in the ascidian central nervous system: revisit to the tripartite model and the origin of the midbrain–hindbrain boundary region. Developmental biology 312, 631-643.
Imai, K.S., Levine, M., Satoh, N., Satou, Y., 2006. Regulatory blueprint for a chordate embryo. Science 312, 1183-1187.
Imai, K.S., Stolfi, A., Levine, M., Satou, Y., 2009. Gene regulatory networks underlying the compartmentalization of the Ciona central nervous system. Development 136, 285-293.
Johnson, C.J., Razy-Krajka, F., Zeng, F., Piekarz, K.M., Biliya, S., Rothbächer, U., Stolfi, A., 2023. Specification of distinct cell types in a sensory-adhesive organ for metamorphosis in the Ciona larva. bioRxiv, 2023.2005.2002.539060.
Jokura, K., Nishino, J.M., Ogasawara, M., Nishino, A., 2020. An α7-related nicotinic acetylcholine receptor mediates the ciliary arrest response in pharyngeal gill slits of Ciona. Journal of Experimental Biology 223, jeb209320.
Lemaire, L.A., Cao, C., Yoon, P.H., Long, J., Levine, M., 2021. The hypothalamus predates the origin of vertebrates. Science Advances 7, eabf7452.
Mazzoni, E.O., Mahony, S., Closser, M., Morrison, C.A., Nedelec, S., Williams, D.J., An, D., Gifford, D.K., Wichterle, H., 2013. Synergistic binding of transcription factors to cell-specific enhancers programs motor neuron identity. Nature neuroscience 16, 1219-1227.
Mendonca, K.d.P., Chaurand, P., Campos, A., Angeletti, B., Rovezzi, M., Delage, L., Borchiellini, C., Bivic, A.L., Issartel, J., Renard, E., Levard, C., 2023. Hyperaccumulation of Vanadium in animals: two sponges compete with urochordates. bioRxiv, 2023.2006.2002.543482.
Nakayama-Ishimura, A., Chambon, J.-p., Horie, T., Satoh, N., Sasakura, Y., 2009. Delineating metamorphic pathways in the ascidian Ciona intestinalis. Developmental biology 326, 357-367.
Nicol, D., Meinertzhagen, I., 1991. Cell counts and maps in the larval central nervous system of the ascidian Ciona intestinalis (L.). Journal of Comparative Neurology 309, 415-429.
Odate, S., Pawlik, J.R., 2007. The role of vanadium in the chemical defense of the solitary tunicate, Phallusia nigra. Journal of chemical ecology 33, 643-654.

Oonuma, K., Yamamoto, M., Moritsugu, N., Okawa, N., Mukai, M., Sotani, M., Tsunemi, S., Sugimoto, H., Nakagome, E., Hasegawa, Y., 2021. Evolution of Developmental Programs for the Midline Structures in Chordates: Insights From Gene Regulation in the Floor Plate and Hypochord Homologues of Ciona Embryos. Frontiers in Cell and Developmental Biology 9, 704367.
Osugi, T., Sasakura, Y., Satake, H., 2020. The ventral peptidergic system of the adult ascidian Ciona robusta (Ciona intestinalis Type A) insights from a transgenic animal model. Scientific Reports 10, 1-11.
Papadogiannis, V., Pennati, A., Parker, H.J., Rothbächer, U., Patthey, C., Bronner, M.E., Shimeld, S.M., 2022. Hmx gene conservation identifies the origin of vertebrate cranial ganglia. Nature 605, 701-705.
Pattyn, A., Hirsch, M., Goridis, C., Brunet, J.-F., 2000. Control of hindbrain motor neuron differentiation by the homeobox gene Phox2b. Development 127, 1349-1358.
Pattyn, A., Morin, X., Cremer, H., Goridis, C., Brunet, J.-F., 1999. The homeobox gene Phox2b is essential for the development of autonomic neural crest derivatives. Nature 399, 366-370.
Petersen, J.K., Mayer, S., Knudsen, M., 1999. Beat frequency of cilia in the branchial basket of the ascidian Ciona intestinalis in relation to temperature and algal cell concentration. Marine biology 133, 185-192.
Picco, V., Hudson, C., Yasuo, H., 2007. Ephrin-Eph signalling drives the asymmetric division of notochord/neural precursors in Ciona embryos.
Razy-Krajka, F., Gravez, B., Kaplan, N., Racioppi, C., Wang, W., Christiaen, L., 2018. An FGF-driven feed-forward circuit patterns the cardiopharyngeal mesoderm in space and time. Elife 7, e29656.
Razy-Krajka, F., Lam, K., Wang, W., Stolfi, A., Joly, M., Bonneau, R., Christiaen, L., 2014. Collier/OLF/EBF-dependent transcriptional dynamics control pharyngeal muscle specification from primed cardiopharyngeal progenitors. Developmental cell 29, 263-276.
Ryan, K., Lu, Z., Meinertzhagen, I.A., 2016. The CNS connectome of a tadpole larva of Ciona intestinalis (L.) highlights sidedness in the brain of a chordate sibling. Elife 5, e16962.
Ryan, K., Lu, Z., Meinertzhagen, I.A., 2017. Circuit homology between decussating pathways in the Ciona larval CNS and the vertebrate startle-response pathway. Current Biology 27, 721-728.
Ryan, K., Meinertzhagen, I.A., 2019. Neuronal identity: the neuron types of a simple chordate sibling, the tadpole larva of Ciona intestinalis. Current opinion in neurobiology 56, 47-60.
Sasakura, Y., Hozumi, A., 2018. Formation of adult organs through metamorphosis in ascidians. Wiley Interdisciplinary Reviews: Developmental Biology 7, e304.
Satija, R., Farrell, J.A., Gennert, D., Schier, A.F., Regev, A., 2015. Spatial reconstruction of single-cell gene expression data. Nature biotechnology 33, 495-502.
Satou, Y., Kawashima, T., Shoguchi, E., Nakayama, A., Satoh, N., 2005. An integrated database of the ascidian, Ciona intestinalis: towards functional genomics. Zoological science 22, 837-843.
Satou, Y., Tokuoka, M., Oda-Ishii, I., Tokuhiro, S., Ishida, T., Liu, B., Iwamura, Y., 2022. A manually curated gene model set for an ascidian, Ciona robusta (Ciona intestinalis type A). Zoological Science 39.
Shi, W., Levine, M., 2008. Ephrin signaling establishes asymmetric cell fates in an endomesoderm lineage of the Ciona embryo.
Shimai, K., Kitaura, Y., Tamari, Y., Nishikata, T., 2010. Upstream regulatory sequences required for specific gene expression in the ascidian neural tube. Zoological science 27, 76-83.
Stolfi, A., Gandhi, S., Salek, F., Christiaen, L., 2014. Tissue-specific genome editing in Ciona embryos by CRISPR/Cas9. Development 141, 4115-4120.
Stolfi, A., Ryan, K., Meinertzhagen, I.A., Christiaen, L., 2015. Migratory neuronal progenitors arise from the neural plate borders in tunicates. Nature 527, 371-374.
Stolfi, A., Wagner, E., Taliaferro, J.M., Chou, S., Levine, M., 2011. Neural tube patterning by Ephrin, FGF and Notch signaling relays. Development 138, 5429-5439.
Stuart, T., Butler, A., Hoffman, P., Hafemeister, C., Papalexi, E., Mauck, W.M., Hao, Y., Stoeckius, M., Smibert, P., Satija, R., 2019. Comprehensive integration of single-cell data. Cell 177, 1888-1902. e1821.

1020 Thompson, E.D., Hogstrand, C., Glover, C.N., 2018. From sea squirts to squirrelfish: facultative trace
1021 element hyperaccumulation in animals. Metallomics 10, 777-793.
1022 Tripathi, D., Mani, V., Pal, R.P., 2018. Vanadium in biosphere and its role in biological processes.
1023 Biological trace element research 186, 52-67.
1024 Ueki, T., Adachi, T., Kawano, S., Aoshima, M., Yamaguchi, N., Kanamori, K., Michibata, H., 2003.
1025 Vanadium-binding proteins (vanabins) from a vanadium-rich ascidian Ascidia sydneiensis samea.
1026 Biochimica et Biophysica Acta (BBA)-Gene Structure and Expression 1626, 43-50.
1027 Ueki, T., Yamaguchi, N., Isago, Y., Tanahashi, H., 2015. Vanadium accumulation in ascidians: a system
1028 overview. Coordination Chemistry Reviews 301, 300-308.
1029 Wada, H., Saiga, H., Satoh, N., Holland, P.W., 1998. Tripartite organization of the ancestral chordate
1030 brain and the antiquity of placodes: insights from ascidian Pax-2/5/8, Hox and Otx genes. Development
1031 125, 1113-1122.
1032 Wang, W., Niu, X., Stuart, T., Jullian, E., Mauck III, W.M., Kelly, R.G., Satija, R., Christiaen, L., 2019. A
1033 single-cell transcriptional roadmap for cardiopharyngeal fate diversification. Nature cell biology 21, 674-
1034 686.

1035